Annu. Rev. Phys. Chem. 2001. 52:681–750

ELECTRON TRANSMISSION THROUGH MOLECULES AND MOLECULAR INTERFACES

Abraham Nitzan
School of Chemistry, The Sackler Faculty of Science, Tel Aviv University, Tel Aviv, 69978, Israel; e-mail: nitzan@post.tau.ac.il

Key Words electron transfer, molecular conduction, molecular electronics, tunneling

■ **Abstract** Electron transmission through molecules and molecular interfaces has been a subject of intensive research due to recent interest in electron-transfer phenomena underlying the operation of the scanning-tunneling microscope on one hand, and in the transmission properties of molecular bridges between conducting leads on the other. In these processes, the traditional molecular view of electron transfer between donor and acceptor species gives rise to a novel view of the molecule as a current-carrying conductor, and observables such as electron-transfer rates and yields are replaced by the conductivities, or more generally by current-voltage relationships, in molecular junctions. Such investigations of electrical junctions, in which single molecules or small molecular assemblies operate as conductors, constitute a major part of the active field of molecular electronics. In this article I review the current knowledge and understanding of this field, with particular emphasis on theoretical issues. Different approaches to computing the conduction properties of molecules and molecular assemblies are reviewed, and the relationships between them are discussed. Following a detailed discussion of static-junctions models, a review of our current understanding of the role played by inelastic processes, dephasing and thermal-relaxation effects is provided. The most important molecular environment for electron transfer and transmission is water, and our current theoretical understanding of electron transmission through water layers is reviewed. Finally, a brief discussion of overbarrier transmission, exemplified by photoemission through adsorbed molecular layers or low-energy electron transmission through such layers, is provided. Similarities and differences between the different systems studied are discussed.

1. INTRODUCTION

Electron transfer, a fundamental chemical process underlying all redox reactions, has been under experimental and theoretical study for many years (1, 2). Theoretical studies of such processes seek to understand the ways in which their rates depend on donor and acceptor properties, on the solvent, and on the electronic coupling between the states involved. The different roles played by these factors

and the way they affect qualitative and quantitative aspects of the electron-transfer process have been thoroughly discussed in the past half-century. These kinds of processes, which dominate electron transitions in molecular systems, are to be contrasted with electron transport in the solid state, i.e. in metals and semiconductors. Electrochemical reactions, which involve both molecular and solid state donor/acceptor systems, bridge the gap between these phenomena (2). Here electron transfer takes place between quasi-free electronic states on one side and bound molecular electronic states on the other.

The focus of this discussion is another class of electron-transfer phenomena: electron transmission between two regions of free or quasifree electrons through molecules and molecular layers. Examples of such processes are photoemission (PE) through molecular overlayers, the inverse process of low-energy electron transmission (LEET) into metals through adsorbed molecular layers, and electron transfer between metal and/or semiconductor contacts through molecular spacers. Figure 1 depicts a schematic view of such systems. The "standard" electron-transfer model in Figure 1*a* shows donor and acceptor sites, with their corresponding polarization wells connected by a molecular bridge. In Figure 1*b* the donor and the acceptor are replaced by a continuum of electronic states representing free space or metal electrodes. (This replacement can occur on one side only, representing electron transfer between a molecular site and an electrode.) In Figure 1*c* the molecular bridge is replaced by a molecular layer. In addition, coupling to the thermal environment may affect transmission through the bridge.

The first two of the examples given above, PE and LEET, involve electrons of positive energy (relative to zero kinetic energy in vacuum) and as such are related to normal scattering processes. The third example, transmission between two conductors through a molecular layer, involves negative energy electrons and as such is closely related to regular electron-transfer phenomena. The latter type of process has drawn particular attention in recent years because of the growing interest in conduction properties of individual molecules and of molecular assemblies. Such processes have become subjects of intensive research because of recent interest in electron-transfer phenomena underlying the operation of the scanning tunneling microscope (STM), and in the transmission properties of molecular bridges between conducting leads. In the latter case, the traditional molecular view of electron transfer between donor and acceptor species gives rise to a novel view of the molecule as a current-carrying conductor, and observables such as electron-transfer rates and yields are replaced by the conductivities, or more generally by current-voltage relationships, in molecular junctions. Of primary importance is the need to understand the interrelationship between the molecular structure of such junctions and their function, i.e. their transmission and conduction properties. Such investigations of electrical junctions, in which single molecules or small molecular assemblies operate as conductors connecting "traditional" electrical components such as metal or semiconductor contacts, constitute a major part of what has become the active field of molecular electronics (3, 4). Their diversity, versatility, and amenability to control and manipulation make molecules and molecular

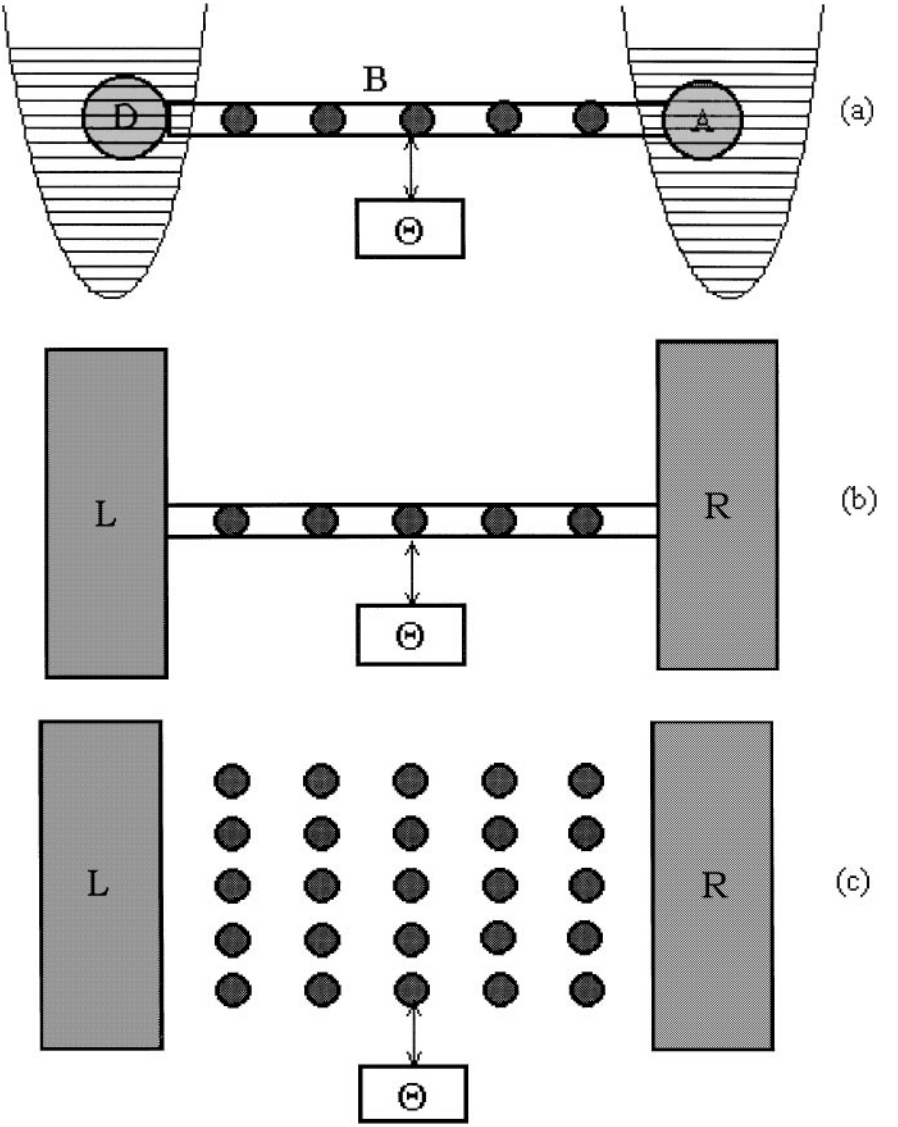

Figure 1 Schematic views of typical electron transmission systems. (*a*) A standard electron-transfer system containing a donor, an acceptor, and a molecular bridge connecting them (not shown are nuclear motion baths that must be coupled to the donor and acceptor species). (*b*) A molecular bridge connecting two electronic continua, L and R, representing e.g. two metal electrodes. (*c*) Same as panel *b* with the bridge replaced by a molecular layer. The Θ blocks represent the thermal environment.

assemblies potentially important components in nano-electronic devices. Indeed, basic properties pertaining to single electron transistor behavior and to current rectification have already been demonstrated. At the same time, major difficulties lie in the way of discovering real technological applications. These difficulties stem from problems associated with the need to construct, characterize, control, and manipulate small molecular structures at confined interfaces with a high degree of reliability and reproducibility, and from issues of stability of such small junctions.

It should be obvious that while the different processes outlined above correspond to different experimental setups, fundamentally they are controlled by similar physical factors. Broadly speaking, we may distinguish between processes for which lifetimes or rates (more generally the time evolution) are the main observables and those that monitor fluxes or currents. In this review, we focus on the second class, which may be further divided into processes that measure current-voltage relationships, mostly near equilibrium, and those that monitor the nonequilibrium electron flux, e.g. in photoemission experiments.

1.0.1 Notations A problem characteristic of an interdisciplinary field such as the one we are covering is that notations that became standard in particular disciplines overlap similarly standard notations of other disciplines. The T operator of scattering theory and the temperature constitute one example; the β parameter of bridge-mediated electron-transfer theory and the inverse (temperature $\times$ Boltzmann constant) is another. I have therefore used nonstandard notations for some variables in order to avoid confusion. Table 1 lists of the main notations used in this article.

2. THEORETICAL APPROACHES TO MOLECULAR CONDUCTION

The focus of this chapter is electron transfer between two conducting electrodes through a molecular medium. Such processes bear strong similarity to the more conventional systems that involve at least one molecular species in the donor/acceptor pair. Still, important conceptual issues arise from the fact that such systems can be studied as part of complete electrical circuits, providing current-voltage characteristics that can be analyzed in terms of molecular resistance, conductance, and capacitance.

2.1 Standard Electron-Transfer Theory

To set the stage for our later discussion, we first briefly review the rate expressions for standard electron-transfer processes (Figures 1*a*, 2*a*). We focus on the particular limit of nonadiabatic electron transfer, where the electron-transfer rate is given

TABLE 1 Notations used

Notation	Variable
T	Scattering operator
$\mathcal{T}$	Transmission coefficient
Θ	Temperature
β	$(k_B\Theta)^{-1}$
β'	Range parameter in electron-transfer rate theory
G	Conduction
σ	Used in different contexts for conductivity and for the reduced system's density operator
I	Current
J	Flux
ρ	Used in different contexts for charge density and for the density operator of the total system
E_F	Fermi energy (E_{FL} and E_{FR} sometimes used for left and right electrodes)
M	Electron electrochemical potential (μ_L and μ_R sometimes used for left and right electrodes)
$\mathcal{F}$	The thermally averaged and Franck-Condon (FC) weighted density of nuclear states
F	System-thermal bath interaction. In specific cases we also use $H_{el\text{-}ph}$
V	Electronic coupling between zero order molecular states
H	System's Hamiltonian
H_B	Bridge Hamiltonian
H_Θ	Hamiltonian of the thermal bath. In some specific cases we also use H_{ph}
Z	Overlap Matrix: $Z_{i,j} = \langle i \mid j \rangle$
$\mathbb{H}$	EZ–H
$\mathcal{H}$	Combined system+thermal bath Hamiltonian
S	S matrix
v	Speed
Φ	Potential or potential difference
Σ	Self energy
Γ	Width (decay rate)
Acronyms	
MMM	Metal-Molecule-Metal (junction)
MIM	Metal-Insulator-Metal (junction)
EH	Extended Huckel
HF	Hartree Fock
FC	Franck-Condon
STM	Scanning tunneling microscope
LEET	Low energy electron transmission
PE	Photoemission

(under the Condon approximation) by the golden rule–based expression

$$k_{et} = \frac{2\pi}{\hbar}|V_{DA}|^2\mathcal{F}, \qquad 1.$$

where V_{DA} is the coupling between the donor (D) and acceptor (A) electronic states and where

$$\mathcal{F} = \mathcal{F}(E_{AD}) = \sum_{\nu_D}\sum_{\nu_A} P_{th}(\varepsilon_D(\nu_D))|\langle\nu_D|\nu_A\rangle|^2\delta(\varepsilon_A(\nu_A) - \varepsilon_D(\nu_D) + E_{AD}), \qquad 2.$$

is the thermally averaged and Franck-Condon (FC) weighted density of nuclear states. In Equation 2, ν_D and ν_A denote donor and acceptor nuclear states, P_{th} is the Boltzmann distribution over donor states, $\varepsilon_D(\nu_D)$ and $\varepsilon_A(\nu_A)$ are nuclear energies above the corresponding electronic origins, and $E_{AD} = E_A - E_D$ is the electronic energy gap between the donor and acceptor states. In the classical limit, $\mathcal{F}$ is given by

$$\mathcal{F}(E_{AD}) = \frac{e^{-(\lambda+E_{AD})^2/4\lambda k_B\Theta}}{\sqrt{4\pi\lambda k_B\Theta}}, \qquad 3.$$

where k_B is the Boltzmann constant, Θ is the temperature, and λ is the reorganization energy, a measure of the electronic energy that would be dissipated after a sudden jump from the electronic state describing an electron on the donor to that associated with an electron on the acceptor. If the donor is replaced by an electrode (2, 5, 6), we have to sum over all occupied electrode states:

$$\begin{aligned}|V_{DA}|^2\mathcal{F} &\Rightarrow \sum_k f(\varepsilon_k)\mathcal{F}(\varepsilon_k - e\Phi)|V_{kA}|^2 \\ &= \int d\varepsilon f(\varepsilon)\mathcal{F}(\varepsilon - e\Phi)\sum_k \delta(\varepsilon - \varepsilon_k)|V_{kA}|^2, \end{aligned} \qquad 4.$$

where

$$f(\varepsilon) = \frac{1}{1 + e^{\varepsilon/k_B\Theta}} \qquad 5.$$

is the Fermi-Dirac distribution function, with ε measured relative to the electron chemical potential μ in the electrode and Φ, which determines the position of the acceptor level relative to μ, is the overpotential. Defining

$$\sum_k \delta(\varepsilon - \varepsilon_k)|V_{kA}|^2 \equiv |V(\varepsilon)|^2, \qquad 6.$$

the electron-transfer rate takes the form

$$k_{et} = \frac{2\pi}{\hbar}\int d\varepsilon \frac{e^{-(\lambda - e\Phi + \varepsilon)^2/4\lambda k_B\Theta}}{\sqrt{4\pi\lambda k_B\Theta}}|V(\varepsilon)|^2 f(\varepsilon). \qquad 7.$$

Note that the reorganization energy that appears in Equation 7 is associated with the change in the redox state of the molecular species only. The nominal change in

the "oxidation state" of the macroscopic electrode does not affect the polarization state of the surrounding solvent because the transferred electron or hole does not stay localized.

Much of the early work on electron transfer has used expressions like those found in Equations 3 and 7, with the electronic coupling term V_{DA} used as a fitting parameter. More recent work has focused on ways to characterize the dependence of this term on the electronic structure of the donor/acceptor pair and on the environment. In particular, studies of bridge-mediated electron transfer, where the donor and acceptor species are rigidly separated by molecular bridges of well-defined structure and geometry, have been very valuable in characterizing the interrelationship between structure and functionality of the separating environment in electron-transfer processes. As expected for a tunneling process, the rate is found to decrease exponentially with the donor-acceptor distance

$$k_{et} = k_0 e^{-\beta' R_{DA}}, \qquad 8.$$

where β' is the range parameter that characterizes the distance dependence of the electron-transfer rate. The smallest values for β' are found in highly conjugated organic bridges for which β' is in the range 0.2–0.6 Å^{-1} (7, 8). In contrast, for free space, taking a characteristic ionization barrier $U_B = 5eV$, we find $\beta' = \sqrt{8mU_B/\hbar^2} \approx 2.4\ \text{Å}^{-1}$ (m is the electron mass). Lying between these two regimes are many motifs, both synthetic and natural, including cytochromes and docked proteins (9, 10), DNA (11–13), and saturated organic molecules (14, 15). Each displays its own characteristic range of β' values, and hence its own timescales and distance dependencies of electron transfer. A direct measurement of β' along a single molecular chain was recently demonstrated (16). In addition to the bridge-assisted transfer between donor and acceptor species, electron transfer has been studied in systems where the spacer is a well-characterized Langmuir-Blodgett film (17). The STM provides a natural apparatus for such studies (16, 18–22). Other approaches include break junctions (23) and mercury drop contacts (24, 25).

Simple theoretical modeling of V_{DA} usually relies on a single electron (or hole) picture in which the donor-bridge-acceptor (DBA) system is represented by a set of levels:$|D\rangle$, $|A\rangle$, $\{|1\rangle, \ldots |N\rangle\}$, as depicted in Figure 2. In the absence of the coupling of these bridge states to the thermal environment, and when the energies E_n ($n = 1, \ldots, N$) are high relative to the energy of the transmitted electron (the donor/acceptor orbital energies in Figures 1*a* and 2*a* or the incident electron energy in Figures 1*b–c* and 2*b*), this is the superexchange model for electron transfer (26). Of particular interest are situations where the states $|1\rangle, \ldots |N\rangle$ are localized in space, so that the state index n corresponds to a position in space between the donor and acceptor sites (Figure 2*a*) or between the two electron reservoirs (Figure 2*b*). These figures depict generic tight-binding models of this type, where the states $n = 1, \ldots, N$ are the bridge states, here taken degenerate in zero order. Their localized nature makes it possible to assume only nearest-neighbor coupling between them, i.e. $V_{n,n'} = V_{n,n\pm1}\delta_{n',n\pm1}$. We recall that the appearance of V_{DA} in Equation 1 is a low-order perturbation theory result. A more

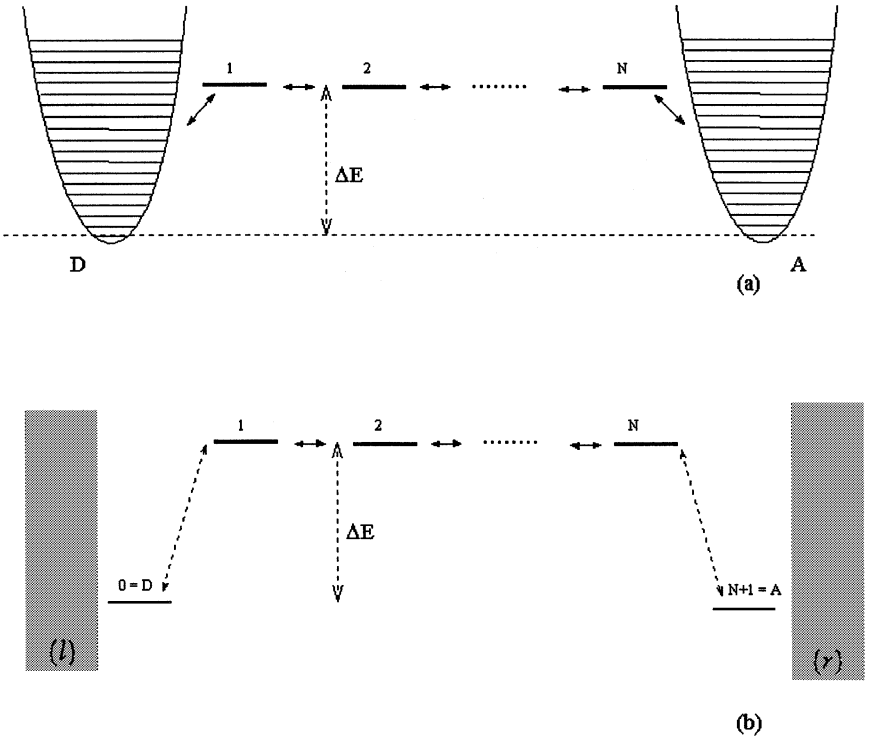

Figure 2 Simple level structure models for molecular electron transfer (*a*) and for electron transmission (*b*). The molecular bridge is represented by a simple set of levels that represents local orbitals of appropriately chosen bridge sites. This set of levels is coupled to the donor and acceptor species (with their corresponding nuclear environments) in panel *a*, and to electronic continua ($\{\ell\}$ for left, {r} for right) representing metal leads in panel *b*. In the latter case, the physical meaning of states 0 and N + 1 depends on the particular physical problem: They can denote donor and acceptor states coupled to the continua of environmental states (hence the notation 0 = D, N + 1 = A), surface localized states in a metal-molecule-metal junction, or belong to the right and left scattering continua.

general expression is obtained by replacing V_{DA} by T_{DA}, where the T operator is defined by $T(E) = V + VG(E)V$, with $G(E) = (E - H + (1/2)i\Gamma)^{-1}$ and where Γ stands for the inverse lifetime matrix of bridge levels. Assuming for simplicity that the donor level $|\mathrm{D}\rangle$ is coupled only to bridge state $|1\rangle$ and that the acceptor level $|\mathrm{A}\rangle$ is coupled only to bridge level N, the effective coupling between donor and acceptor is given by

$$T_{DA}(E) = V_{DA} + V_{D1}G_{1N}(E)V_{NA}. \qquad 9.$$

This naturally represents the transition amplitude as a sum of a direct contribution, V_{DA}, which is usually disregarded for long bridges, and a bridge-mediated

contribution. In using T_{DA} instead of V_{DA} in Equation 1 the energy parameter E in Equation 9 should be taken equal to $E_D = E_A$ at the point where the corresponding potential surfaces cross (or go through an avoided crossing). For the level structure of Figure 2*a* that corresponds to the DBA system in Figure 1*a*, making the tight binding approximation and in the weak coupling limit, $\max|V| \ll \min(E_B - E)$,[1] the Green's function element in Equation 9 is given by

$$G_{1N}(E) = \frac{1}{E - E_N} \prod_{n=1}^{N-1} \frac{V_{n,n+1}}{E - E_n}. \qquad 10.$$

For a model with identical bridge segments, E_n and $V_{n,n+1}$ are independent of n and are denoted $E_n = E_B$ and $V_{n,n+1} = V_B$. Using this in Equation 1 leads to

$$k_{et} = \frac{2\pi}{\hbar} \left| \frac{V_{1D} V_{NA}}{V_B} \right|^2 \left(\frac{V_B}{\Delta E_B} \right)^{2N} \mathcal{F}, \qquad 11.$$

where $\Delta E_B = E_B - E$. Similarly, for a bridge-assisted transfer between a molecule and an electrode, Equation 7 applies, with $|V(\varepsilon)|^2$ given by

$$|V(\varepsilon)|^2 = \left(\frac{V_B}{\Delta E_B} \right)^{2N} \sum_k \delta(\varepsilon - \varepsilon_k) \left| \frac{V_{1k} V_{NA}}{V_B} \right|^2. \qquad 12.$$

These results imply a simple form for the distance parameter β' of Equation 8

$$\beta' = \frac{2}{a} \ln\left(\frac{\Delta E_B}{V_B} \right), \qquad 13.$$

where a measures the segment size, so that the bridge length is Na. The exponential dependence on the bridge length is a manifestation of the tunneling character of this process. For typical values, e.g. $\Delta E_B/V_B = 10$ and a = 5 Å, Equation 13 gives $\beta' = 0.92\ \text{Å}^{-1}$. More rigorous estimates of the electronic coupling term in electron-transfer processes involve electronic-structure calculation for the full DBA system. Such calculations, in the context of molecular conduction, are discussed later.

2.2 Transmission Between Conducting Leads

Equations 1, 7, and 11 are expressions for the rate of electron transfer between donor and acceptor molecules or between a molecule and a metal electrode. As already mentioned, for electron transfer in metal-molecule-metal (MMM) junctions, the primary observable is the current-voltage characteristics of the system. Putting it another way, while the primary observable in standard charge-transfer processes involving molecular donors and/or acceptors is a transient quantity,[2] in

[1]For a generalization of Equation 10 that does not assume weak coupling see Onipko & Klymenko (27).

[2]In addition to rates, other observables are the yields of different products of the electron-transfer reaction.

metal-molecule-metal junctions we focus on the steady-state current through the junction for a given voltage difference between the two metal ends.

Consider first a simple model for a metal-insulator-metal (MIM) system, where the insulator is represented by a continuum characterized by a dielectric constant ε (28). For specificity assume that the electrode surfaces are infinite parallel planes perpendicular to the x direction. In this case, the transmission problem is essentially one dimensional and depends only on the incident particle velocity in the x direction, $v_x = \sqrt{2E_x/m}$. In the WKB approximation, the transmission probability is given by

$$\mathcal{T}(E_x) = \exp\left[-\frac{4\pi}{\hbar}\int_{s_1}^{s_2}[2m(U_B(x) - E_x)]^{1/2}dx\right], \qquad 14.$$

where $U_B(x)$ is the barrier potential that determines the turning points s_1 and s_2 and m is the mass of the tunneling particle. The tunneling flux is given by $\mathcal{T}(E_x)n(E_x)\sqrt{2E_x/m}$, where $n(E_x)$ is the density per unit volume of electrons of energy E_x in the x direction. $n(E_x)$ is obtained by integrating the Fermi-Dirac function with respect to E_y and E_z. When a potential Φ is applied so that the right electrode is positively biased, the net current density is obtained in the form (28)

$$J = \int_0^\infty dE_x \mathcal{T}(E_x)\xi(E_x), \qquad 15.$$

where

$$\xi(E_x) = \frac{2m^2e}{(2\pi\hbar)^3}\int_{-\infty}^{\infty}dv_y\int_{-\infty}^{\infty}dv_z[f(E) - f(E + e\Phi)]$$

$$= \frac{4\pi me}{(2\pi\hbar)^3}\int_0^\infty dE_r[f(E) - f(E + e\Phi)], \qquad 16.$$

and where $E_r = E - E_x = (1/2)m(v_y^2 + v_z^2)$ is the energy in the direction perpendicular to x. In obtaining this result, it is assumed that the electrodes are chemically identical. At zero temperature and when $\Phi \to 0$, $f(E) - f(E + e\Phi) = e\Phi\delta(E - E_F)$. Equations 15 and 16 then lead to an expression for the conduction per unit area, i.e. the conductivity per unit length

$$\sigma_x = \frac{4\pi me^2}{(2\pi\hbar)^3}\int_0^{E_F} dE_x \mathcal{T}(E_x). \qquad 17.$$

For finite Φ, these expressions provide a framework for predicting the current-voltage characteristics of the junction; explicit approximate expressions were given by Simmons (28). Here we only emphasize (28) that the dependence on Φ arises partly from the structure of Equations 15 and 16, for example, at zero temperature,

$$J = \frac{4\pi me}{(2\pi\hbar)^3}\left[e\Phi\int_0^{E_F-e\Phi} dE_x\mathcal{T}(E_x) + \int_{E_F-e\Phi}^{E_F} dE_x(E_F - E_x)\mathcal{T}(E_x)\right], \qquad 18.$$

but mainly from the voltage dependence of $\mathcal{T}$. The simplest model for a metal-vacuum-metal barrier between identical electrodes without an external field is a rectangular barrier of height above the Fermi energy given by the metal workfunction. When a uniform electric field is imposed between the two metals, a linear potential drop from E_F on one electrode to $E_F - e\Phi$ on the other is often assumed. In addition, the image potential experienced by the electron between the two metals will lower the potential barrier (28). This has been invoked to explain the lower-than-expected barrier observed in STM experiments (29). It should be kept in mind that quantum mechanical and atomic size effects, as well as the dynamic nature of the image response, should be taken into account in estimating this correction.

The planar geometry implied by the assumption that transmission depends only on the energy of the motion parallel to the tunneling direction, as well as the explicit form of Equation 14, are not valid for a typical STM configuration that involves a tip on one side and a structured surface on the other. To account for these structures, Tersoff & Hamman (30) have applied Bardeen's formalism (31), which is a perturbative approach to tunneling in arbitrary geometries. Bardeen's formula for the tunneling current is[3]

$$\begin{aligned} I &= \frac{4\pi e}{\hbar} \sum_{l,r} [\, f(E_l)(1 - f(E_r + e\Phi)) \\ &\quad - (1 - f(E_l))\, f(E_r + e\Phi)]|M_{lr}|^2 \delta(E_l - E_r) \\ &= \frac{2\pi e}{\hbar} \sum_{l,r} [\, f(E_l) - f(E_r + e\Phi)]|M_{lr}|^2 \delta(E_l - E_r), \end{aligned} \qquad 19.$$

where

$$M_{lr} = \frac{\hbar^2}{2m} \int d\vec{S} \cdot (\psi_l^* \nabla \psi_r - \psi_l \nabla \psi_r^*) \qquad 20.$$

is the transition-matrix element for the tunneling process. In these equations, ψ_ℓ and ψ_r are electronic eigenstates of the negatively biased (left), and positively biased (right), electrodes, respectively, Φ is the bias potential, and the integral is over any surface separating the two electrodes and lying entirely in the barrier region. The wavefunctions appearing in Equation 20 are eigenfunctions of Hamiltonians that describe each electrode in the absence of the other, i.e interfaced with an infinite spacer medium. These functions therefore decay exponentially in the space between the two electrodes in a way that reflects the geometry and chemical nature of the electrodes and the spacer. For $\Phi \to 0$, Equation 19 yields the

[3]This is just the golden rule rate expression (multiplied by the electron charge e), with M playing the role of coupling. In (30) only the first term in the square brackets of the first line appears. This gives the partial current from the negative to the positive electrode. The net current is obtained by subtracting the reverse current, as shown in Equation 19. Also, compared with (30), Equation 19 contains an additional factor of two that accounts for the spin multiplicity of the electronic states.

conduction

$$g \equiv \frac{I}{\Phi} = \frac{4\pi e^2}{\hbar} \sum_{l,r} |M_{lr}|^2 \delta(E_l - E_F)\delta(E_r - E_F). \quad 21.$$

Tersoff & Hamman (30) have used substrate wavefunctions that correspond to a corrugated surface of a generic metal while the tip is represented by a spherical *s* orbital centered about the center $\mathbf{r}_0$ of the tip curvature. In this case they find

$$I \propto \sum_{\nu} |\psi_\nu(\mathbf{r}_0)|^2 \delta(E_\nu - E_F). \quad 22.$$

The right hand side of Equation 22 is the local density of states of the metal. While this result is useful for analysis of spatial variation of the tunneling current on a given metal surface, the contributions from the coupling matrix elements in Equation 21 cannot be disregarded when comparing different metals and/or different adsorbates (6).

2.2.1 The Landauer Formula The results of Equations 14–17 and 19–21 are special cases of a more systematic representation of the conduction and the current-voltage characteristic of a given junction, as shown by Landauer (32). Landauer's original result was obtained for a system of two one-dimensional leads connecting two macroscopic electrodes (electron reservoirs) via a scattering object or a barrier characterized by a transmission function $\mathcal{T}(\mathrm{E})$. The zero temperature conductance, measured as the limit $\Phi \to 0$ of the ratio I/Φ between the current and the voltage drop between the reservoirs, was found to be[4]

$$g = \frac{e^2}{\pi\hbar}\mathcal{T}(E_F). \quad 23.$$

This result is obtained by computing the total unidirectional current carried in an ideal lead by electrons in the energy range $[(0, E) = (0, \hbar^2 k_E^2/2m)]$. In a one-dimensional system of length L the density of electrons, including spin, with wavevectors in the range between k and $k + dk$, is $n(k)dk = 2(1/L)(L/2\pi) f(E_k)\, dk = f(E_k)dk/\pi$. The corresponding velocity is $v = \hbar k/m$. Thus

$$I(E) = e\int_0^{k_E} dk v(k) n(k) = e\int_0^{k_E} dk(\hbar k/m) f(E_k)/\pi = \frac{e}{\pi\hbar}\int_0^{E} dE' f(E'). \quad 24.$$

At zero temperature, the net current carried under bias Φ is

$$I = \frac{e}{\pi\hbar}\int_0^{\infty} dE(f(E) - f(E + e\Phi)) \xrightarrow{\Theta\to 0} \frac{e^2}{\pi\hbar}\Phi. \quad 25.$$

[4]The corresponding resistance, g^{-1}, can be represented as a sum of the intrinsic resistance of the scatterer itself, $[(e^2/\pi\hbar)(\mathcal{T}/(1-\mathcal{T}))]^{-1}$, and a contribution $(e^2/\pi\hbar)^{-1}$ from two contact resistances between the leads and the reservoirs. [See Chapter 5 of (33) for a discussion of this point.]

Thus the conductance of an ideal one-dimensional lead is $I/\Phi = e^2/\pi\hbar = (12.9K\Omega)^{-1}$. In the presence of the scatterer this is replaced by

$$I = \frac{e}{\pi\hbar}\int_0^\infty dE\mathcal{T}(E)\,(f(E) - f(E+e\Phi)) \xrightarrow{\Theta\to 0,\Phi\to 0} \frac{e^2}{\pi\hbar}\mathcal{T}(E_F)\Phi, \qquad 26.$$

which leads to Equation 23. This result is valid for one-dimensional leads. In cases where the leads have finite size in the direction normal to the propagation so that they support traversal modes, a generalization of Equation 23 yields (33)[5]

$$g = \frac{e^2}{\pi\hbar}\sum_{i,j}\mathcal{T}_{ij}(E_F) = \frac{e^2}{\pi\hbar}\mathbf{Tr}(SS^\dagger)_{E_F}, \qquad 27.$$

where $\mathcal{T}_{ij} = |S_{ij}|^2$ is the probability that a carrier coming from the left, say, of the scatterer in transversal mode i will be transmitted to the right into transversal mode j (S_{ij}, an element of the S matrix, is the corresponding amplitude). The sum in Equation 27 is over all traversal modes whose energy is smaller than E_F. More generally, the current for a voltage difference Φ between the electrodes is given by

$$I = \int_0^\infty dE[f(E) - f(E+e\Phi)]\frac{g(E)}{e}, \qquad 28.$$

$$g(E) = \frac{e^2}{\pi\hbar}\sum_{i,j}\mathcal{T}_{ij}(E). \qquad 29.$$

As an example, consider the case of a simple planar-tunnel junction (see Equations 14–17), where the scattering process does not couple different transversal modes. In this case, the transmission function depends only on the energy in the tunneling direction

$$\sum_{i,j}\mathcal{T}_{ij}(E) = \sum_i \mathcal{T}_{ii}(E) = \frac{L_yL_z}{(2\pi)^2}\int dk_y\int dk_z\mathcal{T}\left[E - (\hbar^2/2m)\left(k_y^2+k_z^2\right)\right]$$

$$= \frac{L_yL_z}{(2\pi)^2}\frac{2\pi m}{\hbar^2}\int_0^E dE_r\mathcal{T}(E-E_r). \qquad 30.$$

E_r is defined below Equation 16. Using this in Equation 27 yields the conductivity per unit length

$$\frac{g}{L_yL_z} \equiv \sigma = \frac{4\pi me^2}{h^3}\int_0^{E_F} dE_x\mathcal{T}(E_x), \qquad 31.$$

in agreement with Equation 17.

[5]The analog of Equation 27 for the microcanonical chemical-reaction rate was first written by Miller (34). Similarly, Equation 32 was first written in a similar context by Miller et al (35).

Similarly, Equations 19 and 21 are easily seen to be equivalent to Equation 23 or 29 if we identify M_{lr} with T_{lr} in Equation 35 below. An important difference between the results of Equations 27–29 and results based on the Bardeen's formalism, Equations 19–21, is that the former are valid for any set of transmission probabilities, even close to 1, whereas the latter yields a weak coupling result. Another important conceptual difference is the fact that the sums over ℓ and r in Equations 19–21 are over zero-order states defined in the initial and final subspaces, whereas the sums in Equations 27–29 are over scattering states, i.e. eigenstates of the exact system's Hamiltonian. It is the essence of Bardeen's contribution (31) that in the weak coupling limit (i.e. high/wide barrier) it is possible to write the transmission coefficient $\mathcal{T}_{ij}$ in terms of a golden rule expression for the transition probability between the zero-order standing-wave states $|l\rangle$ and $|r\rangle$ localized on the left and right electrodes, thus establishing the link between the two representations. [For an alternative formulation of this link, see Galperin et al (36).]

To explore this connection on a more formal basis, we can replace the expression based on transmission coefficients $\mathcal{T}$ by an equivalent expression based on scattering amplitudes, or T matrix elements, between zero-order states localized on the electrodes. This can be derived directly from Equations 27 or 29 by using the identity

$$\sum_{i,j} \mathcal{T}_{ij}(E) = 4\pi^2 \sum_{l,r} |T_{lr}|^2 \delta(E - E_l)\delta(E - E_r). \qquad 32.$$

On the left side of Equation 32 a pair of indices (i,j) denote an exact scattering state of energy E, characterized by an incoming state i on the left, say, electrode and an outgoing state j on the right electrode. On the right, l and r denote zero-order states confined to the left and right electrodes, respectively. T is the corresponding transition operator whose particular form depends on the details of this confinement. Alternatively, we can start from the golden rule–like expression

$$\begin{aligned} I &= e\frac{4\pi}{\hbar} \sum_{l,r} [\, f(E_l)(1 - f(E_r + e\Phi)) \\ &\quad - f(E_r + e\Phi)(1 - f(E_l))]|T_{lr}|^2 \delta(E_l - E_r) \\ &= \frac{4\pi e}{\hbar} \sum_{l,r} [\, f(E_l) - f(E_r + e\Phi)]|T_{lr}|^2 \delta(E_l - E_r). \end{aligned} \qquad 33.$$

(An additional factor of 2 on the right-hand side accounts for the spin degeneracy.) It is convenient to recast this result in the form

$$\begin{aligned} I &= \frac{4\pi e}{\hbar} \int_0^\infty dE[\, f(E) - f(E + e\Phi)] \sum_{l,r} |T_{lr}|^2 \delta(E - E_l)\delta(E - E_r) \\ &= \int_0^\infty dE[\, f(E) - f(E + e\Phi)] \frac{g(E)}{e}, \end{aligned} \qquad 34.$$

where

$$g(E) \equiv \frac{4\pi e^2}{\hbar} \sum_{l,r} |T_{lr}|^2 \delta(E - E_l)\delta(E - E_r). \quad 35.$$

Note that Equations 32 and 35 imply again Equation 29. For $\Phi \to 0$, Equations 34 and 35 lead to $I = g\Phi$, with

$$g = g(E_F). \quad 36.$$

The analogy of this derivation to the result in Equation 21 is evident.

2.3 Molecular Conduction

Equations 34–36 provide a convenient starting point for most treatments of currents through molecular junctions where the coupling between the two metal electrodes is weak. In this case it is convenient to write the system's Hamiltonian as the sum, $H = H_0 + V$, of a part, H_0, that represents the uncoupled electrodes and spacer and the coupling V between them. In the weak coupling limit the T operator

$$T(E) = V + VG(E)V; \quad G(E) = (E - H + i\varepsilon)^{-1} \quad 37.$$

is usually replaced by its second term only. The first "direct" term V can be disregarded if we assume that V couples the states ℓ and r only via states of the molecular spacer. In the simple model (analog of the model that leads to Equation 10) where this spacer is an N-site bridge connecting the two electrodes so that site 1 of the bridge is attached to the left electrodes and site N to the right electrode, we have $T_{lr} = V_{l1}G_{1N}V_{Nr}$. At zero temperature this leads to (37)

$$\sum_{i,j} \mathcal{T}_{ij}(E) = |G_{1N}(E_F)|^2 \Gamma_1^{(L)}(E_F)\Gamma_N^{(R)}(E_F) \quad 38.$$

and, using Equations 34 and 35,

$$I(\Phi) = \frac{e}{\pi\hbar} \int_{E_F - e\Phi}^{E_F} dE |G_{1N}(E, \Phi)|^2 \Gamma_1^{(L)}(E)\Gamma_N^{(R)}(E + e\Phi). \quad 39.$$

Here G_{1N} is an element of the reduced Green's function in the bridge's subspace, obtained by projecting out the metals' degrees of freedom

$$G = (E - H_B - \Sigma_B(E))^{-1}, \quad 40.$$

where $H_B = H_B^0 + V_B$ is the Hamiltonian of the isolated-bridge entity given in the basis of eigenstates of H_B^0 by

$$H_B^0 = \sum_{n=1}^{N} E_n |n\rangle\langle n|; \quad V_B = \sum_{n=1}^{N}\sum_{n'=1}^{N} V_{n,n'} |n\rangle\langle n'|, \quad 41.$$

and where

$$\Sigma_{nn'}(E) = \delta_{n,n'}(\delta_{n,1} + \delta_{n,N})[\Lambda_n(E) - (1/2)i\Gamma_n(E)], \quad 42.$$

$$\Gamma_n(E) = 2\pi \sum_l |V_{ln}|^2 \delta(E_1 - E) + 2\pi \sum_r |V_{rn}|^2 \delta(E_N - E)$$

$$\equiv \Gamma_n^{(L)}(E) + \Gamma_n^{(R)}(E), \quad 43.$$

$$\Lambda_n(E) = \frac{PP}{2\pi} \int_{-\infty}^{\infty} dE' \frac{\Gamma_n(E')}{(E - E')}. \quad 44.$$

The transmission problem is thus reduced to evaluating a Green's function matrix element and two width parameters. The first calculation is a simple inversion of a finite (order N) matrix. The width Γ and the associated shift Λ represent the finite lifetime of an electron on a molecule adsorbed on the metal surface and can be estimated, for example (37), using the Newns-Anderson model of chemisorption (38). In the simple, tight-binding model of the bridge and in the weak coupling limit, G_{1N} is given by Equation 10 modified by the inclusions of the self-energy terms

$$G_{1N}(E) = \frac{V_{1,2}}{(E - E_1 - \Sigma_1(E))(E - E_N - \Sigma_N(E))} \prod_{j=2}^{N-1} \frac{V_{j,j+1}}{E - E_j}. \quad 45.$$

Equations 38–45 thus provide a complete simple model for molecular conduction, equivalent to similar approximations used in theories of molecular electron transfer (e.g. 39 and references therein). Below we discuss more general forms of this formulation.

2.4 Relation to Electron-Transfer Rates

It is interesting to examine the relationship between the conduction of a molecular species and the electron-transfer properties of the same species (40). We should keep in mind that because of tunneling there is always an Ohmic regime near zero bias, with conduction given by the Landauer formula. Obviously this conduction may be extremely low, indicating in practice an insulating behavior. Of particular interest is the estimating of the electron-transfer rate in a given donor-bridge-acceptor (DBA) system that will translate into a measurable conduction of the same system when used as a molecular conductor between two metal leads. To this end consider a DBA system, with a bridge that consists of N identical segments (denoted 1, 2, . . . , N), with nearest neighbor coupling V_B. The electron-transfer rate is given by Equation 11, which we rewrite in the form

$$k_{D\to A} = \frac{2\pi}{\hbar} |V_{D1} V_{NA}|^2 |G_{1N}(E_D)|^2 \mathcal{F}, \quad 46.$$

where, in the weak coupling limit, $|V_B| \ll |E_B - E|$ (see Equation 10)

$$G_{1N}(E) = \frac{|V_B|^{N-1}}{(E_B - E)^N}, \qquad 47.$$

and where $\mathcal{F}$ is the Franck-Condon-weighted density of nuclear states, given in the classical limit by Equation 3. The appearance of $\mathcal{F}$ in Equation 46 indicates that the process is dominated by the change in the nuclear configuration between the two localization states of the electron. Consider now the conduction of a junction where the same DBA complex is used to connect between two metal contacts such that the donor and acceptor species are chemisorbed on the two metals ("left" and "right," respectively). Note that the conduction process does not involve localized states of the electron on the donor or the acceptor, so the factor $\mathcal{F}$ will be absent. Using the model of Section 2.4, we get

$$g(E) = \frac{e^2}{\pi\hbar}|G_{DA}(E)|^2\Gamma_D^{(L)}(E)\Gamma_A^{(R)}(E), \qquad 48.$$

where, in analogy to Equation 45,

$$G_{DA}(E) = \frac{V_{D1}V_{NA}}{(E - E_D - \Sigma_D(E))(E - E_A - \Sigma_A(E))}G_{1N}(E). \qquad 49.$$

Since the donor and acceptor species are chemisorbed on their corresponding metal contacts, their energies shift closer to the Fermi energies, and we therefore assume that the denominator in Equation 49 is dominated by the imaginary parts of the self-energies Σ. Assuming also that the electronic structure of the bridge is not strongly distorted by the proximity to the metals leads to (40)

$$g = g(E_F) = \frac{16e^2}{\pi\hbar}\frac{|V_{D1}V_{NA}|^2}{\Gamma_D^{(L)}(E_F)\Gamma_A^{(R)}(E_F)}|G_{1N}(E_F)|^2;\ E_F = E_D = E_A. \qquad 50.$$

Comparing Equations 6 to Equation 50, we get

$$g = \frac{e^2}{\pi\hbar}\frac{k_{D\to A}}{\mathcal{F}}\frac{8\hbar}{\pi\Gamma_D^{(L)}\Gamma_A^{(R)}}. \qquad 51.$$

In the symmetric case, $E_D = E_A$, we have $\mathcal{F} = (\sqrt{4\pi\lambda k_B T})^{-1}\exp(-\lambda/4k_B T)$. For a typical value of the reorganization energy $\lambda \sim 0.5$ eV, and at room temperature, this is $\sim 0.02\,(\text{eV})^{-1}$. Taking also $\Gamma_D^{(L)} = \Gamma_A^{(R)} \sim 0.5$ eV leads to $g \sim (e^2/\pi\hbar)(10^{-13}k_{D\to A}(s^{-1})) \cong [10^{-17}k_{D\to A}(s^{-1})]\Omega^{-1}$. This sets a criterion for observing Ohmic behavior for small voltage bias in molecular junctions: With a current detector sensitive to pico-amperes, $k_{D\to A}$ has to exceed $\sim 10^6\ \text{s}^{-1}$ (for the estimates of $\mathcal{F}$ and Γ given above) before measurable current can be observed at 0.1-V voltage across such a junction.

2.5 Quantum Chemical Calculations

The simple models discussed above are useful for qualitative understanding of molecular conductivity; however, the Landauer formula or equivalent formulations can be used as a basis for more rigorous molecular calculations using extended Huckel (EH) (20, 21, 41–45) or Hartree Fock (HF) (46–48) calculations. These approaches follow similar semiempirical and ab initio calculations of electron-transfer rates in molecular systems (49). Such atomic-level calculations usually start from a (nonorthogonal) basis set of atomic orbitals, so the formalism described above has to be generalized for this situation.[6] We also relax the assumption that the molecule-metal contact is represented by coupling to a single molecular orbital. Finally, to account for possible strong coupling between the molecular species and the metals, the bridge is usually defined to include small portions of the metals on its two sides. We refer to such a bridge as a supermolecule. Defining the operator

$$\mathbb{H}(E) = EZ - H \text{ with } Z_{ij} = \langle i|j\rangle, \qquad 52.$$

the Green's function is $G(E) = \mathbb{H}(E)^{-1}$. In Equation 52, i and j denote atomic orbitals that may be assigned to the supermolecule (M), the left metal (L), and the right metal (R) subspaces. Denoting formally the coupling between the subspace M and the subspaces $K = L, R$ by the corresponding submatrices $\mathbb{H}_{MK}$, the Green's function for the supermolecule subspace is

$$G^{(M)}(E) = (\mathbb{H} - \Sigma^{(L)} - \Sigma^{(R)})^{-1}, \qquad 53.$$

with[7]

$$\Sigma^{(K)} = \mathbb{H}_{MK}(\mathbb{H}^{-1})_{KK}\mathbb{H}_{KM}. \qquad 54.$$

Using also

$$T_{lr} = \sum_{n,n'} \mathbb{H}_{ln} G_{nn'} \mathbb{H}_{n'r}, \qquad 55.$$

(l and r in the metal L and R subspaces, respectively; n,n' in the supermolecule subspace) in Equation 35 leads to

$$g(E) = \frac{e^2}{\pi\hbar} Tr\left[G^{(M)}(E)\Gamma^{(R)}(E)G^{(M)^\dagger}(E)\Gamma^{(L)}\right], \qquad 56.$$

where, e.g. for the left metal,

$$\Gamma^{(L)}_{n,n'} = 2\pi \sum_l \mathbb{H}_{nl}\mathbb{H}_{ln'}\delta(E - E_l)(n \text{ and } n' \text{ in the molecular subspace}). \qquad 57.$$

In practice, Σ and $\Gamma = -2\mathrm{Im}(\Sigma)$ can be computed by using closure relations based on the symmetry of the metal lattice (42). The trace in Equation 56 is over all basis

[6] Alternatively, it has been shown by Emberly & Kirczenow (50) that one can map the problem into a new Hilbert space in which the basis states are orthogonal.

[7] $\Sigma^{(K)}$ is a matrix in the molecular subspace and Equation 54 is a compact notation for $(\Sigma^{(K)})_{n,n'} = \sum_{k,k'} \mathbb{H}_{nk}(\mathbb{H}^{-1})_{kk'}\mathbb{H}_{k'n'}$, where k and k' are states in the metal K subspace.

states in the (super) molecular subspace. The evaluation of the Green's function matrix elements and of this trace is straightforward in semiempirical single-electron representations such as the extended Huckel approximation, and can be similarly done at the Hartree-Fock level using, after convergence, the Fock rather then the Hamiltonian matrix in Expressions 52–57, and invoking Koopmans' theorem (51). There are obviously considerable weaknesses in these procedures: Both are based essentially on an independent electron (hole) picture, and both are single-electron orbitals associated with the ground-state electronic configuration of the isolated neutral supermolecule. For example, Koopmans' theorem is accurate only for large systems, and the approximation involved in applying it to small systems is one reason why HF is not necessarily superior to EH for calculating the conduction properties of small molecular junctions. [This is true particularly for the lowest unoccupied molecular orbital (LUMO)-dominated conduction, because the HF method is notoriously inadequate for electron affinities while highest occupied molecular orbital (HOMO)-dominated conduction is better represented by this approach; (for further discussion, see 48)].

In spite of these limitations, EH- and HF-based calculations have provided important insight into the conduction properties of molecular junctions. Figure 3 shows a remarkable example. The (EH) calculation is done for a single α,α'-xylyl dithiol molecule adsorbed between two gold contacts. The experiment monitors the current between an STM tip (obtained by cutting a Pt/Ir wire) and a monolayer of such molecules deposited on gold, and it is assumed that lateral interaction between the molecules is unimportant. Two unknown parameters are used for fitting. The first is the position of the metal's Fermi energy in the unbiased junction relative to the molecular energy levels expressed by $E_{FH} \equiv E_F - E_{HOMO}$. The second describes the electrostatic-potential profile along the junction, represented by a parameter η that expresses the distribution of the voltage drop between the two metal leads (see Equation 67 below). As seen in Figure 3, good agreement between theory and experiment is obtained for $E_{FH} = 0.9$ eV and $\eta = 0.5$.

In view of the other unknowns, associated both with the uncertainty about the junction structure and with the simplified computation, the main value of these results is not in the absolute numbers obtained but rather in highlighting the importance of these parameters in determining the junction-conduction behavior. We return to the issue of the junction-potential profile below. Other qualitative issues that were investigated with these types of calculations include the effect of the nature (length and conjugation) of the molecular bridge (41), the effect of the molecule-electrode binding and of the molecular binding site (42), the relation of conductance spectra to molecular electronic structure (52), and the effect of bonding molecular wires in parallel (41, 53).

2.6 Spatial-Grid Based Pseudopotential Approaches

Another way to evaluate the expressions appearing in Equations 32 and 35 as well as related partial sums is closely related to the discrete variable representation

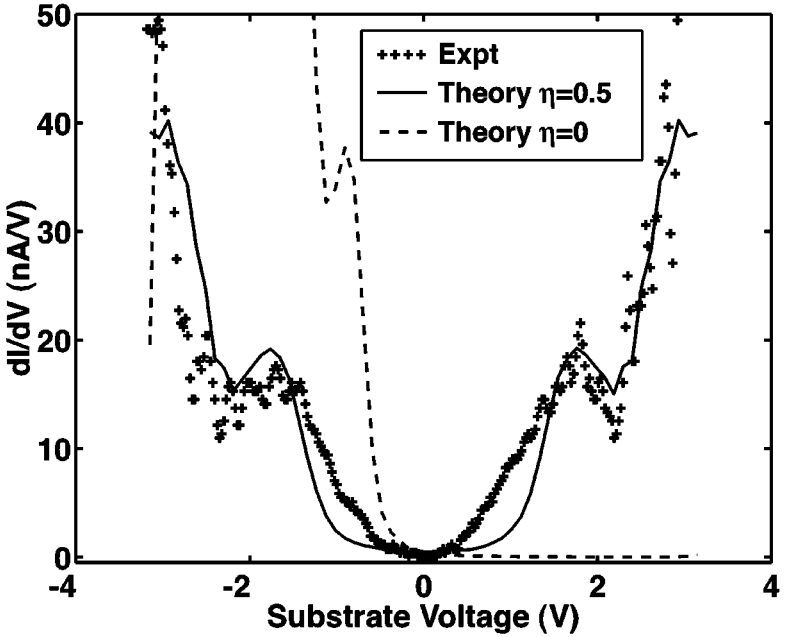

Figure 3 Measured and computed differential conduction of a single α,α'-xylyl dithiol molecule adsorbed between two gold contacts. See text for details. (From Reference 21.)

of reaction probabilities as formulated by Seideman & Miller (54, 54a). We have already seen that the sum

$$s(E) \equiv \sum_{l,r} |T_{lr}|^2 \delta(E - E_l)\delta(E - E_r), \qquad 58.$$

which is related to the conduction by $g(E) = (4\pi e^2/\hbar)s(E)$ (see Equation 35 can be represented by Equation 56).

$$s(E) = \frac{1}{4\pi^2} Tr\left[G^{(M)}(E)\Gamma^{(R)}(E)G^{(M)^*}(E)\Gamma^{(L)}\right]. \qquad 59.$$

If, instead of considering transitions from left to right electrode, we think of Equation 58 as expressing a sum over transition probabilities from all initial (i) states of energy E in the reactant space to all final (f) states of the same energy in the product space, $s(E)$ is also associated with the so-called cumulative reaction probability (34, 54, 54a), which in terms of the reaction S matrix is defined by $N(E) = \sum_{i,f} |S_{if}(E)|^2 = 4\pi^2 s(E)$, i.e. $N(E) = \sum_{i,f} \mathcal{T}_{if}(E)$. Equation 59 now expresses the important observation that the cumulative reaction probability for a reactive scattering process can be expressed as a trace over states, defined in a finite subspace that contains the interaction region, of an expression that depends on the reduced Green's function and the associated self energy defined in that

subspace. Following Seideman & Miller, we can use a spatial grid representation for the states in this subspace, so that the trace in Equation 59 becomes a sum over grid points. Also, in this representation the overlap matrix $\mathbf{Z}$ is zero. In general, any subspace of position space that separates reactants from products (i.e. that encompasses the entire interaction region; the molecular bridge in our application) can be used in Equation 59, provided that the consequences of truncating the "rest of the universe," expressed by the corresponding Σ and Γ, can be computed. The absorbing boundary condition Green's function (ABCGF) method of Seideman & Miller is based on the recognition that if this subspace is shown to be so large that its boundaries are far from the interaction region, the detailed forms of Σ and Γ are not important; the only requirement is that scattered waves that approach these boundaries will be absorbed and not reflected back into the interaction zone. In the ABCGF method, this is accomplished by taking $\Sigma = -(1/2)i\Gamma = -i\varepsilon(\mathbf{r})$, a local function in position space, taken to be zero in the interaction region, and gradually increasing from zero when approaching the subspace boundaries. Its particular form is chosen to affect complete absorption of waves approaching the boundary to a good numerical accuracy. Equation 59 then becomes

$$s(E) = 4Tr\left[G^{ABC}(E)\varepsilon_R G^{ABC^*}(E)\varepsilon_L\right], \qquad 60.$$

where $G^{ABC}(E) = (E - H + i\varepsilon)^{-1}$; $\varepsilon = \varepsilon_R + \varepsilon_L$, and where ε_R and ε_L are different from zero only on grid points near the right side (more generally the product side) and the left (reactant) side of the inner subspace, respectively.

A similar development can be seen for the partial sum

$$s_l(E) \equiv \sum_r |T_{lr}|^2 \delta(E - E_r), \qquad 61.$$

which, provided that l is taken as an eigenstate of the Hamiltonian describing the left electrode (or the reactant sunspace), is related the "one-to-all"–rate, $k_l(E)$, to go from an initial state of energy E on the left electrode (or in reactant space) to all possible states on the right one (product space) according to $k_l = (2\pi/\hbar)s_l$.[8] We use the same definition of the coupling V between our subspace (bridge) and the reactant and product (electrode) states. Putting $T = VGV$ into Equation 61, we get

$$s_l(E) = \frac{1}{2\pi}\langle l|VG^{(M)}\Gamma^{(R)}G^{(M)^*}V|l\rangle. \qquad 62.$$

Using again a position grid representation of the intermediate states to evaluate this expression, and applying the same methodology as above, Equation 62 can be

[8]The "microcanonical rate" is defined by $k(E) = \rho_L^{-1}(E)\sum_l k_l\delta(E - E_l) = (2\pi\hbar\rho_L(E))^{-1}4\pi^2 s(E) = (2\pi\hbar\rho_L(E))^{-1}N(E)$.

recast in the form[9]

$$s_l(E) = \frac{1}{\pi}\langle l|VG^{ABC}(E)\varepsilon_R G^{ABC^*}(E)V|l\rangle$$
$$= \frac{1}{\pi}\langle l|\varepsilon_L G^{ABC}(E)\varepsilon_R G^{ABC^*}(E)\varepsilon_L|l\rangle. \quad 63.$$

The results of Equations 60 and 63 are very useful for computations of transmission probabilities in models where the interaction between the transmitted particle and the molecular spacer is given as a position-dependent pseudopotential. Applications to electron transmission through water and other molecular layers are discussed in Section 4.

2.7 Density Functional Calculations

Density functional methods provide a convenient framework for treating metallic interfaces (55). Applications of this methodology to the problem of electron transport through atomic and molecular bridges have been advanced by several workers. In particular, Lang's approach (56, 57) is based on the density-functional formalism (58) in which the single-electron wavefunctions $\psi_0(\boldsymbol{r})$ and the electron density $n_0(\boldsymbol{r})$ for two bare metal (jellium) electrodes are computed, then used in the Lippman-Schwinger equation

$$\psi(\mathbf{r}) = \psi_0(\mathbf{r}) + \int d\mathbf{r}'d\mathbf{r}''G^0(\mathbf{r},\mathbf{r}')\delta V(\mathbf{r}',\mathbf{r}'')\psi(\mathbf{r}''), \quad 64.$$

to get the full single-electron scattering wavefunctions $\psi(\mathbf{r})$ in the presence of the additional bridge, where G^0 is the Green's function of the bare electrode system and δV is the difference between the potential of the full system containing an atomic or a molecular spacer and that of the bare electrodes. Equation 64 yields scattering states that can be labeled by their energy E, the momentum $\mathbf{k}_\parallel$ in the direction (yz) parallel to the electrodes, the sign, $\pm$, of $\boldsymbol{k}_x$, and the spin. Denoting by μ_L and μ_R the electron-electrochemical potential in the left and right electrode, respectively, the zero-temperature electrical current density from left to right (for $\mu_L > \mu_R$) is then

$$J(\mathbf{r}) = -2\int_{\mu_L}^{\mu_R} dE \int d^2k_\parallel \,\mathrm{Im}\{\psi_+^*\nabla\psi_+\}. \quad 65.$$

The factor 2 accounts for the double occupancy of each orbital. This approach was used recently (59) to calculate current through a molecular species, benzene 1,4-dithiolate molecule [as used in the experiment of Reed et al (19)], between two jellium surfaces and has demonstrated the large sensitivity of the computed current to the microscopic structure of the molecule-metal contacts.

[9]The second part of Equation 63 is obtained by using the identity $\varepsilon_r|l\rangle = 0$ to write $\varepsilon_R G^* V|l\rangle = \varepsilon_R(1 + G^*V)|l\rangle = \varepsilon_R G^*(G^{*-1} + V)|l\rangle$, which, together with $G^{*-1} = E - H_0 - V + i\varepsilon$, $(E - H_0)|l\rangle = 0$, and $\varepsilon|l\rangle = \varepsilon_l|l\rangle$, yields the desired result.

The calculations described above were done in the linear response regime. In contrast, the density-functional approach of Hirose & Tsukada (60) calculates the electronic structure of a metal-insulator-metal system under strong applied bias. This is accomplished by computing the effective one-electron potential in a way that accounts for this bias. This potential contains the standard contributions from the Coulomb and the exchange-correlation interactions as well as from the ionic cores. However, the Coulomb (Hartree) contribution is obtained from the solution of a Poisson equation

$$\nabla^2 V_H(\mathbf{r}) = -4\pi[\rho(\mathbf{r}) - \rho_+(\mathbf{r})], \qquad 66.$$

in the presence of the applied potential-boundary conditions. $\rho_+(\mathbf{r})$ is the fixed positive-charge density, and the electron density $\rho(\mathbf{r})$ is constructed by summing the squares of the wavefunctions over the occupied states. The resulting formalism thus approximately accounts for nonequilibrium effects within the density-functional calculation. A simplified version of the same methodology has recently been presented by Mujica et al (61).

To end this brief overview of density functional-based computations of molecular conduction, we should note that this approach suffers in principle from problems similar to those encountered in using the HF-approximation, namely, the inherent inaccuracy of the computed LUMO energy and wavefunctions. The errors are different, for example, HF overestimates the (HOMO)-LUMO gap [since the HF-LUMO energy is too high (62) whereas DFT underestimates it (63)]. Common to both approaches is the observation that processes dominated by the HOMO level will be described considerably better by these approaches than processes controlled by coupling to the LUMO (48, 64).

2.8 Potential Profiles

The theoretical and computational approaches described above are used to compute both the Ohm-law conduction, $g(E_F)$, of a molecular bridge connecting two metals, (Equation 35 or 56) and the current-voltage characteristics of the junction, also beyond the Ohmic regime (Equation 34). We should keep in mind that these calculations usually disregard a potentially important factor—the possible effect of the imposed electrostatic field on the nuclear configuration as well as on the electronic structure of the bridge. A change in nuclear configuration under the imposed electrostatic field is, in fact, not very likely for stable, chemisorbed molecular bridges. On the other hand, the electronic wavefunctions can be distorted by the imposed field, and this in turn may affect the electrostatic-potential distribution along the bridge,[10] the electronic coupling between bridge segments, and the position of the molecular energy levels vis-à-vis the metal's Fermi energies. These

[10]In a single electron description this local electrostatic potential will be an input, associated with the underlying many-electron response of the molecular bridge, to the position-dependent energies of the bridge electronic states in the site representation.

effects were, in fact, taken approximately into account by Hirose & Tsukada (60) and by Mujica et al (61) by solving simultaneously the coupled Schrödinger and Poisson equations. The latter yields the electrostatic potential for the given electron density and under the imposed potential boundary conditions.

The importance of the electrostatic-potential profile on the molecular bridge in determining the conduction properties of an MMM junction was recently discussed by Tian et al (21) in conjunction with the current-voltage characteristics of a junction comprised of an STM tip, a gold substrate, and a molecule with two bonding sites (e.g. α,α'-xylyl dithiol) connecting the two. For a given potential bias $\Phi = \mu_L - \mu_R$ between substrate (left electrode, for instance) and tip (right electrode), a common model assumption is that the electrostatic potential on the molecule is pinned to that of the substrate so that all the potential drop occurs between the molecule and the tip. In contrast, for MMM junctions with a strong chemical bonding of the molecule to both metals, one often assumes a linear-potential ramp interpolating between the potentials on the two metal leads. In fact, because the molecule is a polarizable object we may expect that most of the potential drop takes place near the molecule-metal contacts (61). Denoting these drops by $\Phi_{\rm L}$ and $\Phi_{\rm R}$ for the left and right electrodes, respectively (so that $\Phi_{\rm L} + \Phi_{\rm R} = \Phi$), the conduction properties of the junction are determined by the position of the molecular-bridge states relative to the equilibrium Fermi energy, and by the voltage division factor η defined by

$$\frac{\Phi_L}{\Phi_R} = \frac{\eta}{1-\eta} \quad \text{or} \quad \eta = \frac{\Phi_L}{\Phi}. \qquad 67.$$

If $\eta = 0$, all the potential drop occurs at the molecule tip (right) interface. In this case, changing the voltage across the junction amounts to changing the energy difference between the molecular levels and the tip electrochemical potential. Enhanced conduction is expected when the latter matches either the HOMO (when the tip is positively biased) or the LUMO (when the tip is negatively biased) energies. However, because the HOMO and the LUMO states are usually coupled differently to the metals (for example, in the aromatic thiols the HOMO is a sulfur-based orbital that couples strongly to the metal whereas the HOMO is a ring-based orbital that couples weakly to it), this implies strong asymmetry, around zero voltage, in the current-voltage dependence, i.e. rectification. In contrast, the observed dependence is essentially symmetric around $\Phi = 0$, a behavior obtained from Equation 34 for a symmetric voltage division factor $\eta = 0.5$ (21).

So far, only a few studies (61, 64) have addressed the computational problem of finding the potential distribution across biased molecular junctions. To what extent the electrostatic potential calculated in these works is relevant for single-electron models of molecular junctions still remains to be clarified. In particular, in other treatments of excess electrons at the insulator side of a metal-insulator interface, the image potential attracting the electron to the interface plays an important role if the insulator dielectric constant is not too large (28, 65). Also, experimental implications of this potential are well known (66). The observation (21) that details

of the electrostatic-potential distribution across an MMM junction can significantly affect qualitative aspects of the junction electrical properties makes further theoretical work in this direction highly desirable.

2.9 Rectification

The possibility of constructing molecular junctions with rectifying behavior has been under discussion since Aviram & Ratner (67) suggested that an asymmetric donor-bridge-acceptor system connecting two metal leads can rectify current. The proposed mechanism of operation of such a device is shown in Figure 4. When the left electrode is negatively biased, i.e. the corresponding electrochemical potentials satisfy $\mu_L > \mu_R$, as shown, electrons can move from this electrode to the LUMO of molecular segment A as well as from the HOMO of molecular segment D to the right electrode. Completion of the transfer by moving an electron from A to D is assisted by the intermediate bridge segment B. When the polarity of the bias is reversed, the same channel is blocked. This simple analysis is valid only if the molecular-energy levels do not move together with the metal electrochemical potentials, and if the coupling through the intermediate bridge is weak enough so

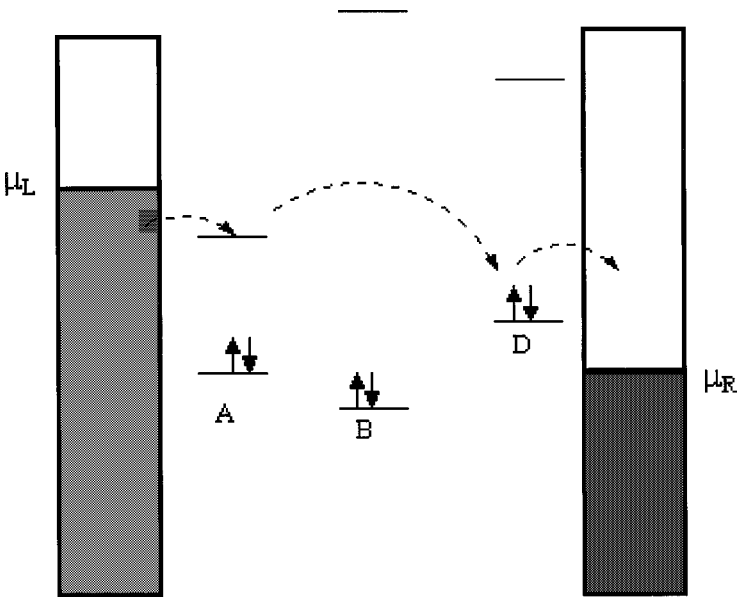

Figure 4 A model for current rectification in a molecular junction. Shown are the chemical potentials μ_L and μ_R in the two electrodes, and the HOMO and LUMO levels of the donor, acceptor, and bridge. When the right electrode is positively biased (as shown), electrons can hop from left to right, as indicated by the dotted arrows. If the opposite bias can be set without affecting the electronic structure of the DBA system too strongly, the reverse current will be blocked.

that the orbitals on the D and A species maintain their local nature. Other models for rectification in molecular junctions have been proposed (68). As discussed above, the expected rectifying behavior can be very sensitive to the actual potential profile in the ABD complex, which in turn depends on the molecular response to the applied bias (21, 69). This explains why rectification is often not observed even in asymmetric molecular junctions (69). Still, rectification has been observed in a number of MMM junctions as well as in several STM experiments involving adsorbed molecules (17, 18, 70, 71).

2.10 Carrier-Carrier Interactions

The models and calculations discussed so far focus on processes for which the probability that a charge carrier occupies the bridge is low so that carrier-carrier interactions can be disregarded. Electron-electron interactions were taken into account only in so far as they affected the single-electron states, either in constructing the molecular spectrum (in the ab initio HF or DFT calculations) or in affecting the junction electrostatic potential through the electronic-polarization response of the molecule or the metal contacts. When the density of carriers in the space between the metal contacts becomes large, Coulomb interactions between them have to be taken into account explicitly. Here we briefly discuss the effect of such interactions.

In classical (hopping) transport of carriers through insulating films separating two metals, intercarrier interactions appear as suppression of current due to film charging (72). In nano-junctions involving double-barrier structures, increased electron population in the intermediate well under resonance transmission should affect the transport process for similar reasons. For example, consider a small metal sphere of radius R in the space between two metal electrodes and assume that both sphere and electrodes are made of the same metal of workfunction W. Neglecting the possible proximity effect of these electrodes, the classical energy for removing an electron from the sphere to infinity is $W + e^2/2R$ and the classical energy for the opposite process is $W - e^2/2R$.[11] Here the sphere plays the role of a molecular bridge in assisting electron tunneling between the two electrodes, and these energies now play the same role as the corresponding HOMO and LUMO energies of the bridge. This implies that a finite voltage difference is needed before current can flow in this sphere-assisted mode between the two metals, a phenomenon known as Coulomb blockade. For a larger potential bias, other conduction channels, corresponding to more highly charged states of the sphere, give rise to the phenomenon of Coulomb steps (74). For experimental manifestations of such and related phenomena (see for instance, 75, 76). The possibility of observing such phenomena in electrochemical systems was discussed by Kuznetsov & Ulstrup (77) and possibly demonstrated by Fan & Bard (78).

[11]From experimental and theoretical work on ionization potentials of small metal clusters (73) we know that the actual energies are approximately $W + 0.4e^2/R$ and $W - 0.6e^2/2R$, respectively, with the differences arising from quantum-size effects.

When the junction consists of a molecule or a few molecules connecting two metal leads, such Coulomb blockade phenomena are not expected to appear so clearly. The first Coulomb threshold is replaced, as just described, by the gap associated with the position of the metal's Fermi energies relative to the molecular HOMO and LUMO levels (modified by appropriate electron correlations). However, the discreteness (in the sense that $\Delta E \gg k_B T$) of the molecular spectrum implies that for any given charging state of the molecule, e.g. a molecule with one excess electron or one excess hole, there will be several distinct conduction channels that will appear as steps in the current vs voltage plot. It will be hard to distinguish between this structure and between a genuine Coulomb blockade structure. It should be emphasized that for potential applications, e.g. using the molecular junction in single-electron transistor devices, the distinction between the origins of these conduction structures is, in principle, not important.

Understanding intercarrier interactions, in particular correlated-carrier transport in molecular junctions, continues to be an important experimental and theoretical challenge. Several recent theoretical works have addressed this problem within the Hubbard model with (79, 80) or without (81) the mean-field approximation. Recent work by Gurvitz & Prager (82), using exactly solvable models of electron transport in two- and three-barrier structures, has indicated that new phenomenology may arise from the interplay of inelastic transitions and intercarrier interactions in the barrier. In fact, dephasing transitions in the barrier may prove instrumental in explaining the charge quantization that gives rise to the single-electron transport behavior of such junctions (see Equation 83, Section 6.3).

2.11 Some Open Issues

This section discusses some subtle difficulties that are glossed over in most treatments of electron transmission using the formalisms described above. These should be regarded as open theoretical issues that should be addressed in the future. The source of these problems is our simplified treatment of what is actually a complex many-body open system. In particular, common ways of incorporating many-body effects using single-body effective potentials becomes questionable in particular limits of timescales and interaction strengths.

One such issue, already mentioned, is the use of a static image to account for the effect of metal polarizability (namely the response of the metal electrons) on charge transfer processes at metal surfaces. The timescales estimated in Section 3.1 below are of the same order as metal-plasma frequencies that measure the electronic-response time of metals. Still, static-image theory has been used in the analysis of Section 2.2 and in other treatments of electron injection from metals into insulating phases (84). To what extent dynamic-image effects are important is not known, although theories that incorporate such effects have been developed (55a).

Assuming that image interactions at metal surfaces should be accounted for in the static limit, namely that the metal responds instantaneously to the tunneling charge, opens other questions. Many calculations of electronic processes near metal

surfaces [e.g. Equation 28; (See Section 2.2 above)] assume that the metal electrons respond instantaneously to the position of the tunneling electron. Other approaches used in different contexts [e.g. reaction-field (cavity) models in quantum chemistry calculations for solvated molecules] calculate the response to electrons in their atomic or molecular orbitals, or, more generally, electronic-charge distributions, and computing these under the given potential-boundary conditions (e.g. see 61) implies that the corresponding orbitals or charge distributions are well defined on timescales shorter than the metal-response times. These two approaches are not equivalent, because the Schrödinger equations derived from them are nonlinear in the electronic wavefunctions. Examination of the energies and timescales involved suggests that in most situations assuming instantaneous metal response to the electron position is more suitable than assuming instantaneous response to the charge distribution defined by a molecular orbital, but the corresponding timescales are not different enough to make this a definite statement. A similar issue appears in attempts to account for the electronic polarizability of a solvent in treating fast electronic processes involving solute molecules or excess electrons in this solvent. We return to this point in Section 4.

Finally, an interesting point of concern is related to the way the Fermi distribution functions enter into the current equations. For example, Bardeen's transmission formula (19) is based on weak coupling between states localized on the two electrodes. Consequently, unidirectional currents contain a product, $f(1-f)$, i.e. the probability that the initial state is occupied multiplied by the probability that the final state is not. In this viewpoint, the transitions occur between two weakly coupled systems, each of them in internal thermal equilibrium, which are out of equilibrium with each other because of the potential bias. Alternatively, we could work on the basis of exact eigenstates of the whole system comprising the two electrodes and the spacer between them. This system is in an internal nonequilibrium state in which transmission can be described as a scattering problem. The relevant eigenstates correspond to incident (incoming) waves in one electrode and transmitted waves in the other. The flux associated with those scattering states arising from an incident state in the negatively biased electrode is proportional to $f(E)$, while that associated with incoming waves in the positively biased electrode is proportional to $f(E + e\Phi)$. The net flux is therefore found again to be proportional to the difference $f(E) - f(E + e\Phi)$. This argument cannot be made unless the process can be described in terms of coherent scattering states defined over the whole system. When inelastic scattering and dephasing processes take place the description in terms of exact scattering states of the whole system becomes complicated (83, 85), although kinetic equations for electron transport can be derived for relatively simple situations (82). On the other hand, it appears that for weakly coupled contacts the perturbative approach that leads to Equation 19 is valid. This approach describes the transmission in terms of electron states localized on the two electrodes where unidirectional rates appear with $f(1-f)$ factors and can, in principle, be carried over to the inelastic regime (see also Section 3.4). The exact correspondence between these different

representation needs further study [see (86) for a recent discussion of experimental implications].

3. DEPHASING AND RELAXATION EFFECTS

The theoretical treatments of electron transmission and conduction through insulating barriers reviewed in the previous section have assumed that the barrier nuclear configuration is static. Consequently, the conduction was computed from the electronic structure of static interfacial configurations. Nuclear reorganization does play a dominant role in the analogous theory of electron transfer in molecular systems; however, here again the electronic coupling itself is computed for static structures, while coupling to nuclear motion is assumed to be associated with the initial and final localized states of the transferred electron. As discussed in Section 2.5, the corresponding nuclear reorganization energies are unimportant in an MMM junction because the transferred electron does not stay localized on the molecular species. Disregarding thermal interactions also during the transmission process therefore leads to a rigid junction model. While we cannot rule out the possible validity of such a model, it is necessary to consider possible scenarios where thermal relaxation on the bridge is important for two reasons. First, dephasing processes associated with electron-phonon coupling are the primary source for converting the transmission process from coherent transfer to incoherent hopping. Therefore ignoring nuclear dynamics disregards a potentially important transfer mechanism. Second, as discussed in the introduction, an important factor in designing molecular conductors is their structural stability; therefore understanding heat generation and dissipation in molecular conductors is an important issue (87, 88). This naturally motivates a study of inelastic effect and thermal relaxation during electron transmission. Indeed, the effect of dephasing and relaxation on carrier transport through molecular junctions (as well as other microscopic charge-transport devices) on its temperature and system-size dependence, and on possible interference effects, has recently attracted much attention.

3.1 Tunneling Traversal Times

The underlying assumption in the treatment of electron transfer and transmission described in Section 2 is that the junction nuclear structure is rigid. The validity of this assumption should be scrutinized. Obviously, whether the barrier appears rigid to the tunneling electron, and to what extent inelastic transitions can occur and affect transmission and conductance, depends on the relative scales of barrier motions and the transmission traversal time, properly defined.

A framework for discussing these issues is the theory of tunneling traversal times. "Straightforward" timescales for tunneling, such as the rate for probability buildup on one side of a barrier following a collision of an incoming particle on

the other side, or the time associated with the tunneling splitting in a symmetric, double-well potential, are important measures of the tunneling rate. Following the work of Büttiker & Landauer (89–91) and others (92), it has been recognized that other timescales may be relevant for other observables associated with the tunneling process. The question of how long the tunneling particle actually spends in the classically forbidden region of the potential is of particular interest. This traversal time for tunneling is useful in estimates of the relative importance of processes that may potentially occur while the particle is in the tunneling region. Energy exchange with other degrees of freedom in the barrier and interaction with external fields focused in the barrier region (e.g. deflection of a tunneling electron by an electrostatic field induced by a heavy ion) are important examples.

The Büttiker-Landauer approach to tunneling timescales is based on imposing an internal clock on the tunneling system, for example a sinusoidal modulation of the barrier height (89). At modulation frequencies much smaller than the inverse-tunneling time, the tunneling particle sees a static barrier that is lower or higher than the unperturbed barrier, depending on the phase of the modulation. At frequencies much higher than the inverse-tunneling time, the system sees an average perturbation and thus no effective change in the barrier height, but inelastic tunneling can occur by absorption or emission of modulation quanta. The inverse of the crossover frequency separating these regimes is the estimated traversal time for tunneling. For tunneling through the one-dimensional rectangular barrier,

$$V(x) = \begin{cases} U_B; & x_1 \le x \le x_2 \\ 0 & otherwise \end{cases}, \qquad 68.$$

and provided that $d = x_2 - x_1$ is not too small, and that the tunneling energy E is sufficiently below U_B, this analysis gives

$$\tau = \frac{d}{v_I} = \sqrt{\frac{m}{2(U_B - E_0)}}d \qquad 69.$$

for a particle of mass m and energy $E_0 < U_B$. v_I, defined by Equation 69, is the imaginary velocity for the under-barrier motion. A similar result is obtained by using a clock based on population transfer between two internal states of the tunneling particle induced by a small barrier-localized coupling between them (90). Using the same clock for electron transfer via the superexchange mechanism in the model of Figure 2 (equal donor and acceptor energy levels, $E_A = E_D$, coupled to opposite ends of a molecular bridge described by an N-state tight-binding model with nearest-neighbor coupling V_B, with an energy gap $\Delta E_B = E_B - E_D \gg V_B$) yields (93)

$$\tau = \frac{\hbar N}{\Delta E_B}. \qquad 70.$$

Nitzan et al (93) have shown that the results in Equations 69 and 70 are limiting

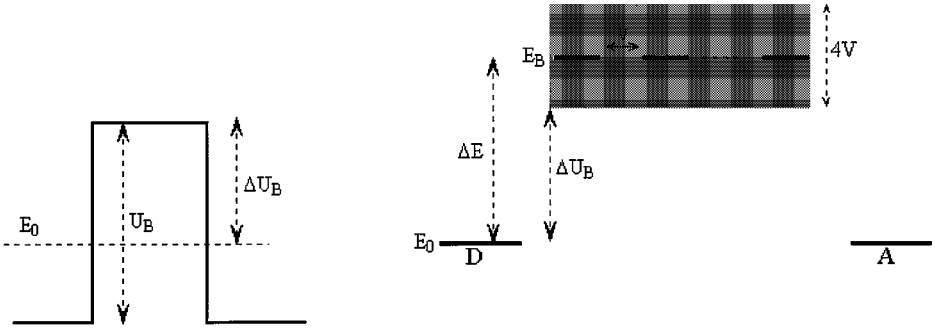

Figure 5 Parameters used in the expressions for tunneling traversal times. *Left*: Tunneling through a rectangular barrier. *Right*: Bridge-mediated transfer, where the gray area denotes the band associated with the tight-binding level structure of the bridge.

cases (wide- and narrow-band limits) of a more general expression

$$\tau = \frac{\bar{h}N}{2V_B\sqrt{\frac{\Delta U_B}{V_B} + \left(\frac{\Delta U_B}{2V_B}\right)^2}}, \qquad 71.$$

where $\Delta U_B \equiv E_B - 2V_B - E_D$ is the difference between the initial energy E_D and the bottom of the conduction band, $E_B - 2V$ (see Figure 5). When $V_B \to 0$, $\Delta U_B \to \Delta E_B$ and the r.h.s of Equation 71 become that of Equation 70. In the opposite limit, $V_B \to \infty$ with ΔU_B kept constant, Equation 71 becomes

$$\tau = \frac{\bar{h}N}{2\sqrt{V_B \Delta U_B}}. \qquad 72.$$

Expressing V_B in terms of the effective mass for the band motion, $m = \bar{h}^2/2V_B a^2$, using $a = d/N$, Equation 72 yields the Büttiker-Landauer result, which is Equation 69.

The interpretation of τ defined above as a characteristic time for the tunneling process should be used with caution. An important observation made by Büttiker (90) is that the tunneling time is not unique but depends on the observable used as a clock. Still, as shown in Büttiker & Landauer (89), for a proper choice of clock the traversal time provides a useful measure for the adiabaticity or nonadiabaticity of the interaction of the tunneling particle with barrier degrees of freedom. The calculation that leads to Equations 70–72 uses a clock based on two internal states, $|1\rangle$ and $|2\rangle$, of the tunneling particle with a small barrier-localized coupling, $\lambda(|1\rangle\langle 2| + |2\rangle\langle 1|)$, between them. The incident particle is in state $|1\rangle$. The population of state $|2\rangle$ in the transmitted wavefunction can be related to the duration of the interstate coupling, i.e. to the traversal time. Writing the transmitted

state in the form $c_1|1\rangle + c_2|2\rangle$ this procedure yields

$$\tau = \lim_{\lambda \to 0} \left(\frac{\hbar}{|\lambda|} \left| \frac{c_2}{c_1} \right| \right). \quad 73.$$

For the one-dimensional rectangular barrier model, Equation 68, and in the limit $\kappa d \gg 1$, this leads again to Equation 69. Galperin et al (94) have applied the same approach to compute traversal times through water layers (see Section 4).

For tunneling through a molecular spacer modeled as a barrier of width ~10 Å (N = 2–3) and height $U_B - E \cong \Delta E \sim 1$ eV, Equations 69 and 70 yield $\tau \cong 0.2$ fs and $\tau \cong 2$ fs, respectively, both considerably shorter than the vibrational period of molecular vibrations. When the barrier is lower or when tunneling is affected or dominated by barrier resonances, the traversal time becomes longer, and competing relaxation and dephasing processes in the barrier may become effective. This is expected to be the rule for resonance transmission through molecular bridges, because the bandwidth associated with the bridge states (i.e. the electronic coupling between them; see Figure 5) is considerably smaller than in metals. As a consequence, thermal relaxation and dephasing are expected to dominate electron transport at and near resonance. This issue is discussed next.

3.2 Nuclear Relaxation During Electron Transmission

It has long been recognized that tunneling electrons interact, and may exchange energy, with nuclear degrees of freedom in the tunneling medium. One realization of such processes is inelastic electron-tunneling spectroscopy (84), where the opening of inelastic channels upon increasing the electrostatic potential difference between the source and sink metals is manifested as a peak in the second derivative of the tunneling current with respect to this potential drop. Recent applications of this phenomenon within scanning-tunneling spectroscopy hold great promise for making the STM a molecular analytical tool (95). Inelastic electron tunneling may also cause chemical bond breaking and chemical rearrangement in the tunneling medium, either by electron-induced consecutive excitation or via transient formation of a negative ion[12] (96).

As discussed by Gadzuk (97), the phenomenology of inelastic electron transmission is also closely related to other electronic processes in which transient occupation of an intermediate state drives a phonon field. Intramolecular vibrational excitation in resonant electron scattering (98), phonon excitation in resonant electron tunneling in quantum-well heterostructures (99, 99a), and electron-induced desorption (100) can all be described using similar models. A prototype Hamiltonian describing these models is

$$H = H_{el} + H_{ph} + H_{el-ph}, \quad 74.$$

[12]While our language refers to electron transport and electron tunneling, hole transport and nuclear excitation via transient positive ion formation are equally possible.

where H_{el} is the electronic Hamiltonian

$$H_{el} = \sum_n E_n c_n^\dagger c_n + \sum_{n,n'(n\neq n')} V_{n,n'} c_n^\dagger c_{n'} + \sum_k E_k c_k^\dagger c_k + \sum_k \sum_n \left(V_{k,n} c_k^\dagger c_n + V_{n,k} c_n^\dagger c_k \right), \quad 75.$$

H_{ph} is the Hamiltonian of the phonon bath

$$H_{ph} = \sum_\nu \hbar\omega_\nu b_\nu^\dagger b_\nu, \quad 76.$$

and H_{el-ph} is the electron-phonon interaction, usually written in the form

$$H_{el-ph} = \sum_n \sum_\nu \lambda_{n\nu} c_n^\dagger c_n \left(b_\nu^\dagger + b_\nu \right). \quad 77.$$

Here $c_j^\dagger$ and $c_j (j = n, n', k)$ create and annihilate an electron in electronic state j, while $b_\nu^\dagger$ and b_ν similarly create and annihilate a phonon of mode ν, of frequency ω_ν. In Equation 75 the states (k) are taken to be different manifolds of continuous-scattering states, denoted by a continuous index k. Figure 2*b* shows two such manifolds, $k = \{\ell\}, \{r\}$, with intermediate states that are discrete electronic states of the observed molecular system. The electronic Hamiltonian (Equation 75) can describe a scattering process in which the electron starts in one continuous manifold and ends in another, and the states {n} belong to the target that causes the scattering process. These states may be the eigenstates of the target Hamiltonian, in which case $V_{n,m}$ in Equation 75 vanishes, or some zero-order representation in which the basis states are mutually coupled by the exact-target Hamiltonian. Equation 76 represents the thermal environment as a harmonic-phonon bath. The coupling between the electronic system and this bath is assumed in Equation 77 to originate from a target-state dependent shift in the equilibrium position of each phonon mode. An exact solution to this scattering problem can be obtained for the particular case where the target is represented by a single state $n = 1$ and the phonon bath contains one oscillator of frequency ω. In this case, it is convenient to consider the oscillator as part of the target that is therefore represented by a set of states $|m\rangle$ with energies $E_1 + m\hbar\omega$ (the zero-point energy can be set to 0). If the oscillator is initially in the ground state ($m = 0$), the cross-section for electron tunneling (or scattering) from left to right is given by (98–99a)

$$\mathcal{T}(E_i, E_f) \sim \Gamma^{(L)}\Gamma^{(R)} \sum_{m'=0}^{\infty} \delta(E_i - E_f - m'\hbar\omega) \times \sum_{\tilde{m}=0}^{\infty} \frac{\langle m'|\tilde{m}\rangle\langle\tilde{m}|0\rangle}{E_i - E_{\tilde{m}} - \Lambda_{\tilde{m}}(E_i) + (i/2)\Gamma_{\tilde{m}}(E_i)}, \quad 78.$$

where $|\tilde{m}\rangle$ are states of the shifted harmonic oscillator that corresponds to the temporary negative ion (electron residing on the target) and $E_{\tilde{m}} = E_1 + m\hbar\omega - \lambda^2/\hbar\omega$. $\Lambda_{\tilde{m}}$ and $\Gamma_{\tilde{m}}$ are the shifts and widths of the dressed-target states associated with

their coupling to the continuous manifolds and

$$\Gamma^{(K)}(E) = 2\pi \sum_k |V_{k,1}|^2 \delta(E - E_k); \quad K = L, k = l \text{ or } K = R, k = r. \quad 79.$$

The exact solution shown in Equation 78 can be obtained because of the simplicity of the system, which was characterized by a single-intermediate electronic state and a single-phonon mode. In more realistic situations characterized by many-bridge electronic states and many-phonon modes, one needs to resort to approximations or to numerical simulations. We discuss such systems next.

To get the proper perspective on the nature of this problem, consider again the standard electron-transfer process in a DBA system without metal electrodes. As already emphasized (see Section 2.5), nuclear dynamics and conversion of electronic energy to nuclear motions, resulting from solvent reorganization about the donor and acceptor sites upon changing their charge state, are essential ingredients of this process. The reason for the prominent role of nuclear dynamics in this case is that the transferred charge is localized on the donor/acceptor orbitals, consequently affecting distortion of their nuclear environments (represented by the parabolas in Figures 1*a* and 2*a*). Standard electron-transfer theory assumes that nuclear motion is coupled to the donor and acceptor electronic states only, and the electronic coupling itself is taken independent of the nuclear configuration (the Condon approximation). This assumption is sometimes questionable, in particular when intermediate electronic states are involved, as in Figures 1 and 2. The possible role of nuclear motion on such intermediate electronic potential surfaces has been discussed by Stuchebrukhov and coworkers (101). Focusing on bridge-assisted, electron-transfer processes, these authors separate the nuclear degrees of freedom into two groups. The first includes those nuclear modes that are strongly coupled to the donor-acceptor system (solvent polarization modes and vibrational modes of the donor and acceptor species). In the absence of the other modes, this coupling leads to the standard electron-transfer rate expression shown by Marcus (see Equations 1, 3 and 9)

$$k_{et} = \frac{2\pi}{\hbar} |T_{DA}|^2 \frac{e^{-(\lambda + E_{AD})^2/4\lambda k_B \Theta}}{\sqrt{4\pi \lambda k_B \Theta}}, \quad 80.$$

where λ is the reorganization energy, E_{AD} is the free-energy difference between the initial (electron on donor) and final (electron on acceptor) equilibrium configurations, and T_{DA} is the nonadiabatic electronic-coupling matrix element that incorporates the effect of the bridge via, for example, Equations 9 and 10. The other group of degrees of freedom, "bridge modes," are coupled relatively weakly to the electron-transfer process, and it is assumed that their effect can be incorporated using low-order perturbation theory. This is accomplished by considering the modulation of the electronic coupling T_{DA} by these motions, $T_{DA} = T_{DA}(\{x_\nu\})$, where $\{x_\nu\}$ is the set of the corresponding nuclear coordinates. It is important to note that the separation of nuclear modes into those coupled to the donor and acceptor states (schematically represented by the Marcus parabolas in Figures 1*a*

and 2a) and those associated with electronic coupling between them is done for convenience only and is certainly not a rigorous procedure. Within this picture the electron-transfer rate is obtained (101) as a convolution

$$k = \int d\varepsilon \rho_B(\varepsilon) k_0(E_{AD} + \varepsilon), \qquad 81.$$

where

$$\rho_B(\varepsilon) = \int dt e^{i\varepsilon t} \frac{\langle T_{DA}(t) T_{DA}(0) \rangle}{\langle T_{DA}^2 \rangle}, \qquad 82.$$

and

$$T_{DA}(t) = e^{iH_B t/\hbar} T_{DA} e^{-iH_B t/\hbar}, \qquad 83.$$

where H_B is the bridge Hamiltonian including the thermal environment ($\Theta\Theta$ of Figure 1). Calculations based on this formalism indicate (101) that inelastic contributions to the total electron-transfer flux are substantial for long (>10 segments) bridges.

It should be emphasized that dynamical fluctuations in the bridge can considerably affect also the elastic transmission probability. For example, a substantial effect of the bridge nuclear motion on the electron-transfer rate has been observed in simulations of electron transfer in aqueous azurin carried out by Xie et al (102), in agreement with earlier theoretical predictions (103). There are some experimental indications that electron-transfer rates in proteins are indeed substantially affected by the protein nuclear motion (104).

Equations 81–83 correspond to the lowest-order correction, associated with intermediate-state nuclear relaxation, for bridge-mediated, electron-transfer rates. At the other extreme, we find sequential processes that are best described by two or more consecutive electronic transitions. For this to happen two conditions have to be satisfied. First, the intermediate state(s) energy should be close to that of the donor/acceptor system, so these states are physically populated either directly or by thermal activation. Second, nuclear relaxation and dephasing should be fast enough so that the bridging states can be treated as well-defined, thermally averaged electronic configurations. Obviously, intermediate situations can exist. Bridge-mediated electron transfer can be dominated by two (donor-acceptor) electronic states coupled via intermediate high-lying states that are only virtually populated, by real participation of such intermediate states in a coherent way (when thermal relaxation and dephasing are slow), or by sequential transfer through such states. This issue was extensively discussed (105, 106) for three-state models of electron transfer that were recently used to describe primary charge separation in bacterial photosynthesis. The possibility of observing similar effects in STM studies of molecules adsorbed at electrochemical interfaces was discussed by Schmickler & Tao (107).

Closely related to this phenomenology is the process of light scattering from molecular systems where the donor and acceptor states are replaced by the incoming and outgoing photons. Elastic (Rayleigh) scattering is the analog of the

two-state standard electron-transfer process. Inelastic (Raman) scattering is the analog of the inelastic electron-transfer process analyzed above, except that our ability to resolve the energy of the scattered photon makes it possible to separate the total rate (or flux), the analog of Equation 81, into its elastic and different inelastic components (108). Resonance Raman scattering and resonance fluorescence are the processes that take place when excited molecular states are physically, as opposed to virtually, occupied during the light-scattering process. The former is a coherent process that takes place in the absence of dephasing and thermal relaxation while the latter follows thermal relaxation in the excited molecular state. Reemitting the photon after dephasing has occurred, but before full thermal relaxation takes place, is the process known as hot luminescence.

3.3 Thermal Interactions in Molecular Conduction

Coming back to electron transfer and transmission, the importance of dephasing effects in the operation of microscopic junctions has long been recognized (33, 83). The Landauer formula for the conduction of a narrow constriction connecting two macroscopic metals, Equations 23 or 27, is derived by assuming that the transmission is elastic and coherent, i.e. without dephasing and energy-changing interactions taking place in the constriction. If the constriction is small relative to the mean free path of the electron in it, these effects may indeed be disregarded. When the constriction becomes macroscopic, multiple scattering and dephasing are essential to obtain the limiting Ohm's law behavior. A simple demonstration is obtained (83, p. 63) by considering a conductor of length L as a series of N macroscopic scatterers, each of the type that, by itself, would yield Equation 23. At each scatterer, the electron can be transmitted with probability $\mathcal{T}$, or reflected with probability $\mathcal{R} = 1 - \mathcal{T}$. Let the total transmission through N such objects be $\mathcal{T}_N$, so that $\mathcal{T} = \mathcal{T}_1$. Provided the phase of the wavefunction is destroyed after each transmission-reflection event, so that we can add probabilities, the transmission through an N-scatterer system is obtained by considering a connection in a series of an $N - 1$ scatterer system with an additional scatterer, and summing over all multiple scattering paths,

$$\mathcal{T}_N = \mathcal{T}_{N-1}(1 + \mathcal{R}\mathcal{R}_{N-1} + (\mathcal{R}\mathcal{R}_{N-1})^2 + \ldots)\mathcal{T} = \frac{\mathcal{T}\mathcal{T}_{N-1}}{1 - \mathcal{R}\mathcal{R}_{N-1}}, \qquad 84.$$

with $\mathcal{R} = 1 - \mathcal{T}$ and $\mathcal{R}_{\mathrm{N}} = 1 - \mathcal{T}_{\mathrm{N}}$. This implies

$$\frac{1 - \mathcal{T}_N}{\mathcal{T}_N} = \frac{1 - \mathcal{T}_{N-1}}{\mathcal{T}_{N-1}} + \frac{1 - \mathcal{T}}{\mathcal{T}} = N\frac{1 - \mathcal{T}}{\mathcal{T}}, \qquad 85.$$

so that

$$\mathcal{T}_N = \frac{\mathcal{T}}{N(1 - \mathcal{T}) + \mathcal{T}} = \frac{L_0}{L + L_0}, \qquad 86.$$

where $L_0 = \mathcal{T}/\nu(1-\mathcal{T})$ and $\nu = N/L$ is the scatterer density. Using this in Equation 23 yields

$$g(E) = \frac{e^2}{\pi\hbar}\frac{L_0}{L+L_0}, \qquad 87.$$

which gives the inverse length-dependence characteristic of Ohm's law as $L \to \infty$ (but see 33, p. 107).

A more detailed treatment of the role played by dephasing in quantum charge transport in microscopic junctions was given by Büttiker (109). He has introduced phase destruction processes by conceptually attaching an electron reservoir onto the constriction, under the condition that, while charge carriers are exchanged between the current-carrying system and the reservoir, no net-averaged current is flowing into this reservoir. Büttiker has observed that such a contact, essentially a voltage probe, acts as a phase-breaking scatterer. By adjusting the coupling strength between this device and the system, a controlled amount of incoherent current can be made to be carried through the system. This approach has been very useful in analyzing conduction properties of multigate junctions and connected nano-resistors.

In molecular systems, a very different approach to dephasing was considered by Bixon & Jortner (110), who pointed out that the irregular nature of Franck-Condon overlaps between intramolecular vibrational states associated with different electronic centers can lead to phase erosion in resonant electron transfer. Consequently, bridge-assisted electron transfer, which proceeds via the superexchange mechanism in off-resonance processes, will become sequential in resonance situations. For a finite temperature system with an electronic energy gap between donor and bridge that is not too large relative to $\kappa_B\Theta$, the thermally averaged rate from a canonical distribution of donor states results in a superposition of both superexchange and sequential mechanisms.

While coupling to the thermal environment is implicit in the models described above, using molecular bridges embedded in condensed environments as conductors immediately suggests the need to consider the coupling to intramolecular and environmental nuclear motions explicitly, as in the Hamiltonian shown in Equations 74–77. The models of Figures 1 and 2, where transition between the two electron reservoirs or between the donor and acceptor species is mediated by a bridge represented by the group of states {n}, are again the starting point of our discussion. Several workers have recently addressed the theoretical problem of electron migration in such models, where the electron is coupled to a zero-temperature phonon bath. Bonča & Trugman (111, 111a) have provided an exact numerical solution for such a problem. Their model is similar to that described by Equations 74–77, except that the metal leads connected to the molecular target are represented by one-dimensional, semi-infinite, tight-binding Hamiltonians:

$$H = H_{el} + H_{ph} + H_{el-ph}, \qquad 88.$$

$$H_{el} = \sum_n E_n c_n^\dagger c_n + \sum_k E_k c_k^\dagger c_k + \sum_{n,n'} V_{n,n'} c_n^\dagger c_{n'} + \sum_{k,k'} V_{k,k'} c_k^\dagger c_k + \left(\sum_{n,k} V_{n,k} c_n^\dagger c_k + h.c \right), \quad 89.$$

$$H_{ph} = \sum_\nu \hbar\omega_\nu b_\nu^\dagger b_\nu, \quad 90.$$

$$H_{el-ph} = \sum_n \sum_\nu \lambda_{n\nu} c_n^\dagger c_n (b_\nu^\dagger + b_\nu). \quad 91.$$

Here, H_{el} desribes both the metal leads [represented by the manifold(s) of states {k}] and the molecular target (with states {n}). The coupling to the phonon field is assumed to vanish on the metal sites. The electron transport problem is treated as a one-particle, multichannel scattering problem, where each of the (one incoming, many outgoing) channels corresponds to a given vibrational state of the target. A finite basis is employed by using a finite number of phonon modes and limiting the number of phonons quanta associated with each site, and by projecting out leads that carry only outgoing states; however, the size of this basis can be increased until convergence is achieved. Yu et al (112) have studied the same one-dimensional electronic model with a different electron-phonon interaction: Instead of the Holstein-type interaction, as seen in Equations 77 and 91, they use a model similar to the Su-Schrieffer-Heeger (SSH) Hamiltonian (113), where Equations 89–91 are replaced by

$$H_{el} + H_{el-ph} = \sum_n E_n c_n^\dagger c_n + \sum_n \left\{ [V_{n,n+1} - \alpha_{n,n+1}(u_{n+1} - u_n)] c_n^\dagger c_{n+1} + h.c. \right\}, \quad 92.$$

$$H_{ph} = \frac{1}{2} K \sum_{n=1}^{N-1} (u_{n+1} - u_n)^2 + \frac{1}{2} \sum_{n=1}^{N} m_n \dot{u}_n^2, \quad 93.$$

where $u_n (n = 1, \ldots, N)$ are displacements of the target atoms. The segment of the lattice between $n = 1$ and $n = N$ represents an organic oligomer, connecting between two metals, and the model for the oligomer is the same as that used in the SSH theory of conducting conjugate polymers, with the nuclear degrees of freedom treated classically. The electron-phonon coupling is again assumed to vanish outside the bridge, i.e. in Equation 92, $\alpha_{n,n+1}$ is taken to be zero unless $n = 1, 2, \ldots, N - 1$. A special feature (in the context of this review) of this calculation is that it is done using the exact many-electron ground state of the metal-oligomer-metal system, which takes into account the Peierls distortion that leads to a dimerization in the oligomer's structure (113). The time evolution of an excess-electron wavepacket going through the oligomer segment is computed using the quantum-classical, time-dependent, self-consistent field (TDSCF) approximation, whereupon the electron wavefunction is propagated under the instantaneous

nuclear configuration, while the latter is evolved classically using the expectation value of the Hamiltonian with the instantaneous electronic wavefunction.[13] It was found that lattice dynamics can be quite important at an intermediate window of electron energies, where the electronic and nuclear timescales are comparable.

A fully quantum analog of this model was studied by Ness & Fisher (114). Their Hamiltonian is

$$H_{el} = \sum_n E_n c_n^\dagger c_n + \sum_\nu \hbar\omega_\nu b_\nu^\dagger b_\nu + \sum_{\nu,n,m} \gamma_{\nu,n,m}\left(b_\nu^\dagger + b_\nu\right) c_n^\dagger c_m, \qquad 94.$$

where, again, the distinction between the metal leads and the molecular system enters through the values of the site energies E_n, and through the fact that coupling to phonons exists only at the oligomer sites. The ground state of the neutral N electron-dimerized chain is the reference system, and the time evolution in the corresponding $N + 1$ or $N - 1$ electron system is studied at zero temperature using the multichannel, time-independent scattering-theory approach of Bonča & Trugman (111, 111a). The result of this calculation is a considerable increase in the tunneling current when the electron-phonon interaction is switched on, in particular for long chains. The origin of this behavior seems to be the existence of a polaron state below the conduction band edge of the molecular segment that effectively lowers the barrier energy experienced by the tunneling electron. Close to resonance, however, the effect of electron-phonon coupling may be reversed, leading to a smaller total overall conduction (115).

The Bonča & Trugman approach (111, 111a) has also been used recently by Emberly & Kirczenow (85), also for a one-dimensional, tight-binding model described by the SSH Hamiltonian. These authors attempt to take into account the Pauli exclusion principle in calculating the inelastic contributions to electron transmission and reflection. While the formalism can, in principle, be applied to finite temperature processes, the implementation is done for a low-temperature system. The result again indicates that inelastic processes can substantially modify electron transport for long molecular chains and large potential drops.

3.4 Reduced Density Matrix Approaches

The research described above uses models for quantum transport that yield practically exact numerical solutions at the cost of model simplicity: one-dimensional, tight-binding transport models; only a few harmonic oscillators; and essentially zero temperature systems. An alternative approach uses the machinery of nonequilibrium statistical mechanics, starting from a Hamiltonian such as in Equation 88 and projecting out the thermal bath part. The resulting reduced equations of motion for the electronic subsystem contain dephasing and energy-relaxation rates that are related explicitly to properties of the thermal-bath and the system-bath coupling.

[13]An open issue in this calculation is the validity of the TDSCF approximation. This approximation is known to be problematic in tunneling and scattering calculations where the quantum wavefunction splits to several distinct components.

Such approaches to bridge-mediated electron transport were made by several workers (116–119). For simplicity we limit ourselves to the tight-binding superexchange model for bridge-mediated electron transfer (see Section 2.1). Also, for simplicity of notation we consider N bridge states between the two electrodes, without assigning special status to donor and acceptor states, as in Figure 2*b*. (It should be obvious that this makes only a notational difference.) The Hamiltonian for the athermal system is

$$H = H_0 + V, \tag{95.}$$

$$H_0 = \sum_{n=1}^{N} E_n|n\rangle\langle n| + \sum_l E_l|l\rangle\langle l| + \sum_r E_r|r\rangle\langle r|, \tag{96.}$$

$$V = \sum_l (V_{l,1}|l\rangle\langle 1| + V_{1,l}|1\rangle\langle l|) + \sum_{n=1}^{N-1}(V_{n,n+1}|n\rangle\langle n+1| + V_{n+1,n}|n+1\rangle\langle n|) + \sum_r (V_{r,N}|r\rangle\langle N| + V_{N,r}|N\rangle\langle r|), \tag{97.}$$

where $\{l\}$ and $\{r\}$ are again continuous manifolds corresponding to the left and right metal leads and $\{n\}$ is a set of bridge states connecting these leads in the way specified by the corresponding elements of the coupling V. In the absence of thermal interactions, and when the left and right electrodes are coupled only to levels 1 and N of the bridge, respectively, transport in this system is descibed by the conduction function (see Equations 29 and 38)

$$g(E) = \frac{e^2}{\pi\hbar}|G_{1N}(E)|^2\Gamma_1^{(L)}(E)\Gamma_N^{(R)}(E), \tag{98.}$$

with

$$\Gamma_1^{(L)}(E) = 2\pi\sum_l |V_{l1}|^2\delta(E_1 - E); \quad \Gamma_N^{(R)}(E) = 2\pi\sum_r |V_{Nr}|^2\delta(E_N - E). \tag{99.}$$

In general, $G(E)$ is evaluated numerically by inverting the corresponding Hamiltonian matrix. For $E_n = E_B$ and $V_{n,n+1} = V_B$, identical for all bridge levels and for all mutual couplings, respectively, and in the superexchange limit, $|V_B| \ll |E_B - E|$, the Green's function element is $V_B^{N-1}/\Delta E_B^N$ (see Equation 10), with $\Delta E_B = E - E_B$. In this case, g depends exponentially on the bridge length N according to $g \sim \exp[-\beta' N]$ with $\beta' = 2\ln(|\Delta E_B/V_B|)$ (see Equation 13).

3.4.1 Weak Thermal Coupling To see how these dynamics are modified by thermal relaxation and dephasing effects, we follow the formulation of Segal et al (118) The Hamiltonian H is supplemented by terms describing a thermal-bath and a system-bath interaction

$$\mathcal{H} = H + H_\Theta + F, \tag{100.}$$

where H_Θ is the Hamiltonian for the thermal environment or bath, and where the system-bath interaction F is assumed weak. In this case, thermal coupling between

different bridge levels is neglected relative to the internal coupling V between them, so

$$F = \sum_{n=1}^{N} F_n |n\rangle\langle n|, \qquad 101.$$

where F_n are operators in the bath degrees of freedom that satisfy $\langle F_n \rangle \equiv Tr_\Theta (e^{-\beta H_\Theta} F_n) = 0$ (Tr_Θ is a trace over all thermal bath states). F is characterized by its time-correlation function. As a simple model we postulate

$$\langle F_n(t) F_{n'}(0) \rangle = f(t)\delta_{n,n'}. \qquad 102.$$

The Fourier transform of the remaining correlation functions satisfies the detailed balance condition,

$$\int_{-\infty}^{\infty} dt e^{i\omega t} \langle F_n(t) F_n(0) \rangle = e^{\beta\hbar\omega} \int_{-\infty}^{\infty} dt e^{i\omega t} \langle F_n(0) F_n(t) \rangle; \beta = (k_B\Theta)^{-1}, \qquad 103.$$

where Θ is the temperature and β is the Boltzmann constant. For specificity we sometimes use

$$f(t) = \frac{\kappa}{2\tau_c} \exp(-|t|/\tau_c), \qquad 104.$$

which becomes $\kappa\delta(t)$ in the Markovian, $\tau_c \to 0$, limit. Note that Equation 101 is a particular model for the thermal interactions, sufficient to show their general consequences, but by no means adequate for quantitative predictions. In particular, the assumption in Equation 102 will be replaced by a more realistic model below.

Galperin et al (36) have shown that the conduction properties of a system like that described by the Hamiltonian Equations 95–100 can be obtained by studying a steady state in which the amplitude of one state $|0\rangle$ in the initial $\{l\}$ manifold remains constant and the amplitudes of other states evolve under this restriction. Segal et al (118) have generalized this approach to thermal systems of the kind described by the Hamiltonian Equation 100 using, in the weak thermal-coupling limit, the Redfield approximation (116, 120). This approximation combines two steps that rest on the weak-coupling limit: an expansion up to second order in the coupling F and the assumption that the thermal bath is not affected by its coupling to the molecular system. In this approach, one starts from the set of states $|0\rangle, |1\rangle, \ldots, |n\rangle, \{|l\rangle\}, \{|r\rangle\}$, where $|0\rangle$ is the incoming state in the $\{l\}$ manifold, and projects out the continuous manifolds $\{l\}$ (except $|0\rangle$) and $\{r\}$. This amounts to replacing H of Equations 95–100 by an effective Hamiltonian, H^{eff}, in the space spanned by states $|0\rangle, |1\rangle, \ldots, |n\rangle$, in which the energies E_1 and E_N are modified by adding self-energy terms whose imaginary parts are, respectively, $\Gamma_1^{(L)}/2$ and $\Gamma_N^{(R)}/2$. This effective Hamiltonian of order $N+1$ is then diagonalized and the resulting set of $N+1$ states (originating from N bridge states and one incoming state) is used to represent the Liouville equation for the density operator ρ of the overall electrode-bridge-bath system, $\dot{\rho} = -i[\mathcal{H}, \rho]$. This Liouville equation

is expanded to second order in F and traced over bath degrees of freedom using the approximation $\rho(t) = \rho_\Theta \sigma(t)$, with $\rho_\Theta = e^{-\beta H_\Theta}$ and $\sigma(t) = Tr_\Theta \rho(t)$. This leads to an equation of motion for the reduced density matrix $\sigma(t)$ for the electrode-bridge system that takes the form

$$\begin{aligned}\dot{\sigma}_{jk} = &-iE_{jk}\sigma_{jk} - \Gamma_{jk}\sigma_{jk} \\ &- \int_0^t dt' \sum_{lm} \{\langle \tilde{F}_{jl}(t-t')\tilde{F}_{lm}(0)\rangle e^{-iE_{lk}(t-t')}\sigma_{mk}(t') \\ &- \langle \tilde{F}_{mk}(0)\tilde{F}_{jl}(t-t')\rangle e^{-iE_{kl}(t-t')}\sigma_{lm}(t') \\ &- \langle \tilde{F}_{mk}(t-t')\tilde{F}_{jl}(0)\rangle e^{-iE_{jm}(t-t')}\sigma_{lm}(t') \\ &+ \langle \tilde{F}_{ml}(0)\tilde{F}_{lk}(t-t')\rangle e^{-iE_{jl}(t-t')}\sigma_{jm}(t')\}, \end{aligned} \quad 105.$$

where $E_{jl} = E_j - E_l$ and $\tilde{F}(t) = e^{iH_\Theta t} F e^{-iH_\Theta t}$. Here the indices j,k,l,m refer to molecular states that diagonalize the effective Hamiltonian H_{eff}. The damping terms Γ originate from the decay of states $|1\rangle$ and $|N\rangle$ distributed into these eigenstates. At steady state all σ elements are constant and Equation 105 becomes

$$\begin{aligned}0 = &-iE_{jk}\sigma_{jk} - \Gamma_{jk}\sigma_{jk} \\ &+ \sum_{lm} \left\{ \sigma_{lm} \int_0^\infty d\tau \left(\left\langle \tilde{F}_{mk}(0)\tilde{F}_{jl}(\tau)\right\rangle e^{-iE_{lk}\tau} + \left\langle \tilde{F}_{mk}(\tau)\tilde{F}_{jl}(0)\right\rangle e^{-iE_{jm}\tau}\right) \right. \\ &- \sigma_{mk} \int_0^\infty d\tau \langle \tilde{F}_{jl}(\tau)\tilde{F}_{lm}(0)\rangle e^{-iE_{lk}\tau} \\ &\left. -\sigma_{jm} \int_0^\infty d\tau \langle \tilde{F}_{ml}(0)\tilde{F}_{lk}(\tau)\rangle e^{-iE_{jl}\tau} \right\}. \end{aligned} \quad 106.$$

Transforming Equation 106 back to the local bridge representation $\{0, n = 1, \ldots, N\}$ leads to a set $(N+1)(N+1)$ equations of the form

$$-iE_{nn'}\sigma_{nn'} - i[V,\sigma]_{nn'} + \sum_{n_1}\sum_{n_2} R_{nn'n_1n_2}\sigma_{n_1n_2} = \frac{1}{2}(\Gamma_n + \Gamma_{n'})\sigma_{nn'};$$

$$n, n' = 0, \ldots, N, \quad 107.$$

where the elements of R are linear combinations of the integrals appearing in Equation 106 and where $\Gamma_n = \Gamma_N^{(R)}\delta_{n,N} + \Gamma_1^{(L)}\delta_{n,1}$. Again, at steady state the first $(n = n' = 0)$ equation is replaced by the boundary condition $\sigma_{00} =$ constant. The remaining $(N+1)(N+1)-1$ equations constitute a set of linear nonhomogeneous algebraic equations in which the terms containing σ_{00} constitute source terms.

Thus, all elements $\sigma_{nn'}$, and in particular σ_{NN}, can be obtained in the form $\sigma_{nn'} = U_{nn'}\sigma_{00}$, in terms of the fixed population σ_{00} in the incoming state $|0>$ of the $\{l\}$ manifold, where the coefficients $U_{nn'}$ are related to the inverse of the $(N+1)$ $(N+1)-1$ order matrix of thermal rates. The steady state flux into the $\{r\}$ manifold is $\Gamma_N^{(R)}\sigma_{NN}$, and the corresponding rate is

$$k_{0\to R} = \Gamma_N^{(R)}\sigma_{NN}/\sigma_{00} = \Gamma_N^{(R)}U_{NN}. \qquad 108.$$

While the general expression for U_{NN} is very cumbersome, involving the inverse of an $(N+1)(N+1)-1$ order matrix, numerical evaluation of the resulting rate and its dependence on coupling parameters, bridge length, and temperature is an easy numerical task for reasonable bridge lengths. A final technical point stems from the observation that the resulting $k_{0\to R}$ must be proportional to $|V_{10}|^2$, the squared coupling between the first bridge level and the left continuous manifold. We therefore rewrite Equation 108 in terms of new variables $k'_{0\to R}$ and U'_{NN}, defined by

$$k_{0\to R} = k'_{0\to R}|V_{10}|^2 = \Gamma_N^{(R)}U'_{NN}|V_{10}|^2. \qquad 109.$$

We can make contact with results obtained in the athermal case by writing $|0\rangle = |k_\parallel, k_x\rangle$, where x is the direction of transmision, $k_\parallel$ is the momentum in the yz plane, and $(\hbar^2/2m)(k_\parallel^2 + k_x^2) = E_\parallel + E_x = E_0$. The transmission coefficient $\mathcal{T}(E_0, k_\parallel)$ for electron incident from the left electrode with total energy E_0 in channel $k_\parallel$ is related to $k_{0\to R}$ by

$$k_{0\to R} = \frac{k_x}{mL}\mathcal{T}(E_0, k_\parallel) = (2\pi\rho(E_x))^{-1}\mathcal{T}(E_0, k_\parallel), \qquad 110.$$

where $\rho(E_x)$ is the one-dimensional density of states for the motion in the x direction. Therefore,

$$\mathcal{T}(E_0, k_\parallel) = 2\pi\rho(E_x)k_{0\to R} = \Gamma_{1,k_\parallel}^{(L)}k'_{0\to R}, \qquad 111.$$

and the all-to-all transmission at energy E_0 is the sum over all channels with energy $E_\parallel < E_0$

$$\mathcal{T}(E_0) = \Gamma_1^{(L)}k'_{0\to R} = \Gamma_1^{(L)}\Gamma_N^{(R)}U'_{NN}. \qquad 112.$$

Comparing Equation 112 with Equation 98, we see that Equation 112 is the analog of Equation 38, where, in the thermal case, U'_{NN} has replaced $|G_{1N}|^2$.

In the athermal case, the conduction of a junction characterized by a given transmission coefficient is obtained from the Landauer formula (27). Here the issue is more complex since, while $\mathcal{T}(E_0)$ is the probability that an incident electron with energy E_0 will be transmitted through the molecular barrier, it is obvious that the transmitted electron can carry energy different from E_0. As an example, consider the case where the bridge has only one intermediate state, i.e. $N = 1$. Within the same model and approximations as outlined above, it is possible (121)

to obtain the energy-resolved transmission. In the Markovian limit ($\tau_c \to 0$ in Equation 104) the result is

$$\mathcal{T}'(E_0, E) = \mathcal{T}_0(E_0)\left[\delta(E_0 - E) + \frac{(\kappa/2\pi)e^{-\beta(E_1-E_0)}}{(E_1 - E)^2 + (\Gamma_1/2)^2}\right], \qquad 113.$$

[we use $\mathcal{T}'$ to denote the differential (per unit energy range) transmission coefficient], where $\Gamma_1 = \Gamma_1^{(L)} + \Gamma_1^{(R)}$ and $\mathcal{T}_0$ is elastic transmission coefficient

$$\mathcal{T}_0(E_0) = \frac{\Gamma_1^{(L)}\Gamma_1^{(R)}}{(E_1 - E_0)^2 + (\Gamma_1/2)^2}.$$

The total transmission coefficient, including inelastic contribution, is given by

$$\mathcal{T}(E_0) = \int dE\mathcal{T}'(E_0, E) = \mathcal{T}_0(E_0)\left[1 + \frac{\kappa}{\Gamma_1}e^{-\beta(E_1-E_0)}\right]. \qquad 114.$$

In the absence of thermal interactions ($\kappa = 0$ in Equation 104), $\mathcal{T}$ is reduced to $\mathcal{T}_0$, and the electron is transmitted with $E = E_0$. For a finite κ we get an additional, thermally activated, component peaked around the energy E_1 of the bridge level.

How will this affect the conduction? It has been argued (see 83) that simple expressions based on the Pauli principle (e.g. Equations 19 and 33) are not valid in the presence of inelastic processes, including thermal relaxation. It may still be used however in the weak metal-bridge coupling limit (see discussion in Section 2.12). Proceeding along this line, an equation equivalent to Equation 33 can be written

$$I = \frac{e}{\pi\hbar}\int_0^\infty dE_0 \int_0^\infty dE\mathcal{T}'(E_0, E) \times [f(E_0)(1 - f(E + e\Phi)) - f(E_0 + e\Phi)(1 - f(E)]. \qquad 115.$$

For small bias and low enough temperature [so that $f(E + e\Phi) \sim f(E) - e\Phi\delta(E - E_F)$], this leads to (121)

$$g(E_0) = \frac{I}{\Phi} = \frac{e^2}{\pi\hbar}\mathcal{T}_0(E_0)\left(1 + (1 - f(E_1))\frac{\kappa}{\Gamma_1}e^{-\beta(E_1-E_0)}\right). \qquad 116.$$

The equivalent result for electron-transfer rates is familiar: At zero-temperature, the rate is determined by a tunneling probability, and at higher temperature an activated component takes over. For an experimental manifestation of this behavior (e.g. see 122, Figure 5).

It is also interesting to examine the bridge-length dependence of the transfer rate and the associated conduction. Here analytical results are cumbersome, but numerical evaluation of the rate (Equation 108), and the transmission coefficients (Equations 111 and 112), in terms of the system parameters (Hamiltonian

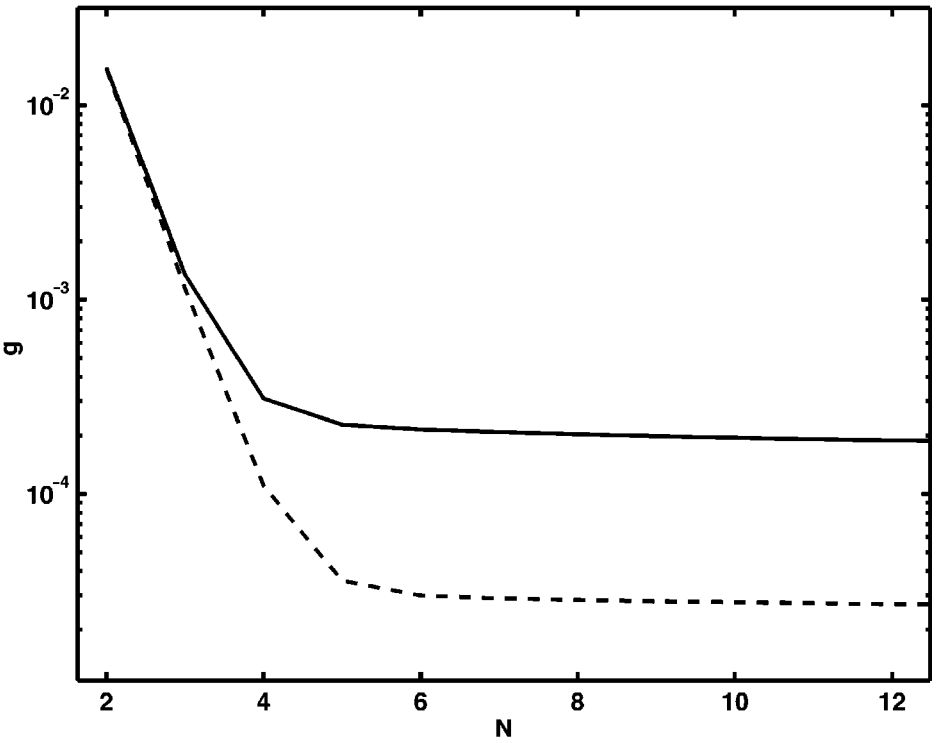

Figure 6 Finite temperature conduction of a simple tight-binding model of a molecular junction as a function of bridge length *N*. (See text for details.)

couplings and the parameters κ and τ_c of Equation 104) is straightforward (118). Figure 6 shows the conduction (in units of $e^2/\pi\hbar$) obtained from such a model calculation using $V_B = 0.05\,\text{eV}$, $\Delta E_B = E_B - E_F = 0.2\,\text{eV}$, $\Gamma_l^{(L)} = \Gamma_N^{(R)} = 0.1\,\text{eV}$, $\tau_c = 0$, $\kappa = 0.01$ eV, plotted against the number of bridge segments N for two different temperatures, $T = 300$ K and 500 K. An exponential dependence on N, characteristic of the superexchange model, is seen to give way to a weak bridge-length dependence at some crossover value of N. Further analysis of these results (118, 119) reveals that the dependence on bridge length beyond the crossover may be written in the form $(k_{up}^{-1} + k_{diff}^{-1}N)^{-1}$, where k_{up} is the rate associated with the thermal-activated rate from the Fermi-level into the bridge, whereas k_{diff} corresponds to hopping (diffusion) between bridge sites. As N increases, the conduction behaves as N^{-1}, indicating Ohmic behavior. This inverse length dependence should be contrasted with nondirectional diffusion, where the rate to reach a distance N from the starting position behaves like N^{-2}. Furthermore, if other loss channels exist, carriers may be redirected or absorbed with a rate

TABLE 2 Bridge-length dependence of the transmission rate (118)

Physical Process	Bridge-length (N) dependence	
Super exchange (*small N, large* $\Delta E_B/V_B$, *large* $\Delta E_B/\kappa_B\Theta$)	$e^{-\beta' N}$	$\beta' = 2\ln(V_B/\Delta E_B)$
Steady state hopping (*large N, small* $\Delta E_B/V_B$, *small* $\Delta E_B/k_B\Theta$)	N^{-1}	
Nondirectional hopping (*large N, small* $\Delta E_B/V_B$, *small* $\Delta E_B/k_B\Theta$)	N^{-2}	
Intermediate range (*intermediate N, small* $\Delta E_B/V_B$)	$(k_{up}^{-1} + k_{diff}^{-1} N)^{-1}$	$k_{up} \sim (V_B{}^2\kappa/\Delta E^2)e^{-\Delta E_B/k_B\Theta}$ $k_{diff} \sim (4V_B{}^2/\kappa)e^{-\Delta E_B/k_B\Theta}$
Steady state hopping + competing loss at every bridge site	$e^{-\alpha N}$	$\alpha = \sqrt{\Gamma_B(\Gamma_B + \kappa)}/2V_B$

Γ_B once they populate the bridge, the bridge-length dependence again becomes exponential and may be written $g \sim (k_{up}^{-1} + k_{diff}^{-1}N)^{-1}e^{-\alpha N}$, where α is related to this loss rate (13, 123). Table 1 (118) summarizes these results for the Markovian limit of the thermal-relaxation process.

Experimental observation of the behaviors indicated in Table 2 is not easy since it is usually not possible to change the length of a molecular bridge without affecting its other properties, e.g. the positions of molecular HOMOs and LUMOs relative to donor and acceptor energies or an electrode Fermi energy (124). A nice example (125) of a crossover behavior observed in a LEET experiment (see Section 6) as a function of thickness of an absorbed molecular layer is seen in Figure 7. Here electrons are injected into N-hexane films adsorbed on a polycrystaline Pt foil at energies below the bottom of the conduction band ($\sim$0.8 eV). The role of bridge states is here assumed by impurity states in the hydrocarbon band gap. Since the energy and localization position of these states is not known, the observed results cannot be quantitatively analyzed with the model described above. However, a crossover from tunneling to hopping behavior is clearly seen.

3.4.2 Strong Thermal Coupling The weak system-thermal, bath-coupling model discussed above rests on two approximations: (*a*) The system-bath interaction can be considered in low order, and (*b*) the bath degrees of freedom are essentially unaffected by the electronic process. Using these assumptions has enabled us to obtain the general characteristics of electron transmission through

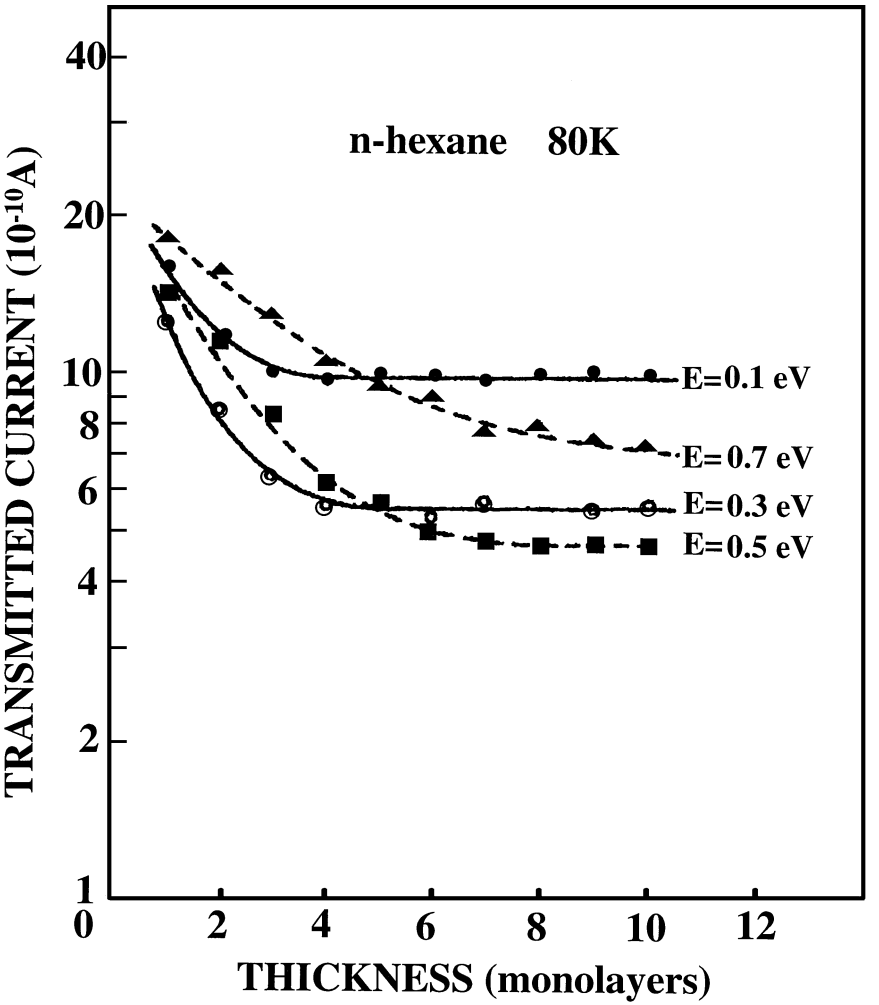

Figure 7 Transmitted current in n-hexane films as a function of thickness for various incident energies, showing the transition from tunneling to activation-induced transport. (Reproduced from Reference 125 and used by permission.)

molecular barriers in the presence of barrier-localized thermal interactions. When the interaction between the electronic system and the underlying bath is stronger, these assumptions break down, and distortions in the bath configuration induced by the electronic process can play an important role. One example is the analysis of Ness & Fisher (114) discussed above, where coupling to phonons increases the overall transmission because of the existence of a polaron state below the

conduction band edge of the electronic system. However, because the overall transmission efficiency depends both on energetics (the polaron state lowers the effective barrier height) and coupling strength (small nuclear overlaps between distorted and undistorted nuclear configurations decreases the effective coupling), the issue is more involved, and depending on details of coupling and frequencies, both enhancement or reduction of transmission probabilities can occur. Similarly, at finite temperatures, the relative importance of the two transmission routes, tunneling and activated hopping, is sensitive to these details. Relatively simple results are obtained in the particular limit where the thermal coupling is strong while the bare electronic-coupling V_B is weak. In this case, it may still be assumed that the bath degrees of freedom remain in thermal equilibrium throughout the process. Taking the bath to be a system of harmonic oscillators, $H_B = \sum_\alpha [(p_\alpha^2/2m_\alpha) + (m_\alpha \omega_\alpha^2/2)x_\alpha^2]$, and taking F_n in Equation 101 to be linear in the coordinates x_α,

$$F_n = (1/2)\sum_\alpha C_{n\alpha} x_\alpha \qquad 117.$$

(so that the Hamiltonian used in Equation 100 is similar to the polaron-type Hamiltonian used in Equations 74–77 and 88–91), a small polaron transformation is applied in the form

$$\begin{aligned} \mathcal{H}' &= U\mathcal{H}U^{-1} \\ U &= U_1 U_2 \ldots U_N \\ U_n &= \exp(-|n\rangle\langle n|\Omega_n) \\ \Omega_n &= \sum_\alpha \Omega_{n\alpha}; \quad \Omega_{n\alpha} = \frac{C_{n\alpha} p_\alpha}{2m_\alpha \omega_\alpha^2}, \end{aligned} \qquad 118.$$

leading to the transformed Hamiltonian

$$\begin{aligned} \mathcal{H}' &= H + H_B + F' + E_{shift} \\ F' &= V_B \sum_{n=1}^{N-1} \left(|n\rangle\langle n+1| e^{i(\Omega_{n+1}-\Omega_n)} + |n+1\rangle\langle n| e^{-i(\Omega_{n+1}-\Omega_n)} \right) \\ E_{shift} &= -\frac{1}{8}\sum_n \sum_\alpha \frac{C_{n\alpha}^2}{m_\alpha \omega_\alpha^2} |n\rangle\langle n|, \end{aligned} \qquad 119.$$

where H is given by Equations 95–97. If V_B is small, the procedure based on the Redfield approximation, which leads to Equation 107, can be repeated. Note that keeping terms only up to second order in F′ still includes terms of arbitrary order in the system-bath coupling. This procedure leads to (D Segal, A Nitzan,

unpublished result)

$$\dot{\sigma}_{jk} = -i\omega_{jk}\sigma_{jk} - iV_B \sum_m \left(\langle F'_{jm}\rangle\sigma_{mk} - \langle F'_{mk}\rangle\sigma_{jm}\right)$$
$$+ V_B^2 \sum_{l,m} \left\{ \sigma_{lm} \int_0^\infty d\tau \left(\langle \tilde{F}_{mk}(0)\tilde{F}_{jl}(\tau)\rangle e^{-iE_{lk}\tau} + \langle \tilde{F}_{mk}(\tau)\tilde{F}_{jl}(0)\rangle e^{-iE_{jm}\tau}\right)\right.$$
$$\left. - \sigma_{mk} \int_0^\infty d\tau \langle \tilde{F}_{jl}(\tau)\tilde{F}_{lm}(0)\rangle e^{-iE_{lk}\tau} - \sigma_{jm} \int_0^\infty d\tau \langle \tilde{F}_{ml}(0)\tilde{F}_{lk}(\tau)\rangle e^{-iE_{jl}\tau}, \right. \quad 120.$$

where $\tilde{F} = F' - \langle F'\rangle$. The terms in the first line of Equation 120 account for coherent motion with a modified coupling operator, while the terms proportional to $V_B{}^2$ describe incoherent hopping between bridge sites. An important new element in this formulation is the temperature-dependent renormalization of the coupling responsible for the coherent transmission. Using Equation 119 results in

$$\langle F'\rangle = \exp(-S_T)$$
$$S_T = (1/2)\sum_\alpha d_{n\alpha}^2(2\overline{n}_\alpha + 1)$$
$$\overline{n}_\alpha = (\exp(\omega_\alpha/k_BT) - 1)^{-1}$$
$$d_{n\alpha}^2 = \frac{(C_{n\alpha} - C_{n+1,\alpha})^2}{8m_\alpha\omega_\alpha^3}, \quad 121.$$

so that coherent transfer becomes less important at higher temperatures. This reduction in the coherent hopping rate is associated with the small overlap between bath degrees of freedom accommodating the electron at different sites. In fact, $\langle F'\rangle$ is recognized as the thermally averaged Franck-Condon factor associated with the electron transfer between two neighboring bridge sites. In terms of the spectral density

$$J(\omega) = \frac{\pi}{2}\sum_\alpha \frac{(C_{n\alpha} - C_{n+1,\alpha})^2}{m_\alpha\omega_\alpha}\delta(\omega - \omega_\alpha) \quad 122.$$

(independent of n if the bridge sites are equivalent), we have

$$S_T = \frac{1}{8\pi}\int_0^\infty \frac{J(\omega)\coth(\omega/2k_BT)}{\omega^2}d\omega \xrightarrow[\text{finite } T]{\omega\to 0} \frac{k_BT}{4\pi}\int_0^\infty \frac{J(\omega)}{\omega^3}d\omega. \quad 123.$$

Depending on the spectral density, this integral may diverge. More specifically, if $J(\omega) \sim \omega^s$ with $s < 2$, S_T diverge at any finite temperature and the coherent route is blocked. In other cases, the coherent route quickly becomes insignificant with increasing temperature.

We have extended this discussion of thermal relaxation and dephasing effects in bridge-assisted electron transport both because these effects are inherently important in determining transport and conduction properties of molecular junctions, and because the issue of heat generation in these current-carrying nanostructures is intimately related to these relaxation phenomena. As we have seen, this problem is far from being solved and more research along these lines can be expected.

4. ELECTRON TUNNELING THROUGH WATER

Electron tunneling through water is obviously an important element in all electron-transfer processes involving hydrated solutes and in many processes that occur in water-based electrochemistry. Still, only a few systematic experimental studies of the effect of the water structure on electron-transfer processes have been done (22, 24, 126–131). Porter & Zinn (24) have found, for a tunnel junction made of a water film confined between two mercury droplets, that at low (<1 nm) film thickness, conduction reflects the discrete nature of the water structure. Nagy (130) has studied STM current through adsorbed water layers and has found that the distance dependence of the tunneling current depends on the nature of the substrate and possibly indicates the existence of resonance states of the excess electron in the water layer. Vaught et al (129) have seen a nonexponential dependence on tip-substrate distances of tunneling in water, again indicating that at small distances water structure and possibly resonance states become important in affecting the junction conductance. Several workers have found that the barrier to tunneling through water is significantly lower than in a vacuum for the same junction geometry (22, 126–128, 130, 131). The observed barrier is considerably lower than the threshold observed in photoemission into water (132) and, in contrast to tunneling in a vacuum, cannot be simply explained by image effects (24).

The present section focuses on attempts (133–138) to correlate these observations with numerical and theoretical studies. In the spirit of most calculations of electron-transfer rates (as in Section 2) and of earlier dielectric continuum modes that neglect water structure altogether, we assume at the outset that in films consisting of a few monolayers, transmission is dominated by elastic processes. The discussion in Section 3 emphasizes the need to justify this assumption. Since we are dealing with negative-energy (tunneling) processes, electronic excitations of water molecules by the transmitting electron can be ruled out. In addition, photoemission through thin water films adsorbed on metals indicates that inelastic processes associated with the water's nuclear motion contributes relatively weakly at such energies (139). Numerical simulations of subexcitation electron transmission through 1–4 water monolayers adsorbed on Pt (1,1,1) (140) are in agreement with this observation.[14] Theoretical calculations of inelastic tunneling (144)

[14]It should be kept in mind that energy transfer from the transmitting electron to water, nuclear degrees of freedom, the mechanism responsible for capturing and localizing the electron as a solvated species, must play an important role for thicker layers (141–143).

similarly show that sufficiently far from resonance, the overall transmission is only weakly affected by inelastic processes. In both cases, this can be rationalized by the short interaction times (see 140; see also Section 3.1). In such cases, a static medium assumption appears to provide a reasonable starting point for discussing the overall transmission, i.e. we assume that the transmission event is completed before substantial nuclear motion takes place. The computation of the transmission probability can therefore be done for individual static water configurations sampled from an equilibrium ensemble, and the results averaged over this ensemble. This assumption is critically examined below. It should be emphasized that while solvent nuclear motion is slow relative to the transmission timescale, solvent electronic response (electronic polarizability) is not. We return to this issue below.

In Section 2 we have summarized the theoretical and computational approaches available for studying electron transfer and electron transmission. The following account (see also 137) summarizes recent computational work on electron transmission through water that uses the pseudopotential method (133–136, 138). Here the detailed information about the electronic structure of the molecular spacer is disregarded and replaced by the assumption that the underlying electron scattering or tunneling can be described by a one-electron potential surface. This potential is taken to be a superposition of the vacuum potential experienced by the electron and the interaction potential between an excess electron and the molecular spacer. The latter is written as a sum of terms representing the interaction between the electron and the different atomic (and sometimes other suitably chosen) centers. The applicability of this method depends on our ability to construct reliable pseudopotentials of this type. In the work described below, we use the electron-water pseudopotential derived and tested in studies of electron hydration (145); [for an alternative pseudopotential, see Rossky & Schnitker (145a)], and a modified pseudopotential that includes the many-body interaction associated with the water electronic polarizability.

With such a potential given, the problem is reduced to evaluating the transmission probability of an electron when it is incident on the molecular layer from one side only. In recent years, various time-dependent and time-independent numerical-grid techniques were developed for such calculations. In the time-dependent mode, an electron wavepacket is sent toward the molecular barrier and propagated on the grid using a numerical solver for the time-dependent Schrödinger equation. This propagation continues until such time t_f at which the collision with the barrier has ended, i.e. until the probability that the electron is in the barrier region, $\int_{barrier} |\psi(\mathbf{r}, t)|^2 d\mathbf{r}$, has fallen below a predetermined margin. Since only the result at the end of the time evolution is needed, a propagation method based on the Chebychev polynomial expansion of the time-evolution operator (146) is particularly useful.

In the time-independent mode, Nitzan and coworkers (137, 147) have applied the spatial-grid–based, absorption-boundary condition, Green's-function (ABCGF) technique described in Section 2.7 (Equations 60 and 63). Taking x to be the tunneling direction, periodic boundary conditions are used in the y–z plane

parallel to the molecular layer, and the absorption function, $\varepsilon(\boldsymbol{r}) = \varepsilon(x)$, is taken to be different from zero near the grid boundaries in the z direction, far enough from the interaction region (i.e. the tunneling barrier), and gradually diminishing to zero as the interaction region is approached from the outside. The stability of the computed transmission to moderate variations of this function provides one confidence test for this numerical procedure. The cumulative microcanonical transition probability and the one-to-all transition rates are calculated as outlined in Section 2.7. In addition, exact outgoing and incoming wavefunctions Ψ_i^+ and Ψ_f^-, which correspond to initial and final states (eigenfunctions of H_0 with energy E) ϕ_i and ϕ_f, respectively, can be computed from

$$\psi_i^+ = \frac{1}{E - H + i\varepsilon} i\varepsilon\phi_i$$
$$\psi_f^- = \frac{1}{E - H - i\varepsilon}(-i\varepsilon)\phi_f, \qquad 124.$$

and provide a route for evaluating state-selected transition probabilities, $S_{if} = \langle\psi_f^-|\psi_i^+\rangle$. The evaluation of these expressions requires (*a*) evaluating the Hamiltonian matrix on the grid, and (*b*) evaluating the operation of the corresponding Green's operator on a known vector. As in most implementations of grid Hamiltonians, the resulting matrix is extremely sparse, which suggests the applicability of Krylov space-based iterative methods (148).

Although considerable sensitivity to the water structure is found in these studies, water layers prepared with different reasonable water-water interaction models have similar transmission properties (134, 135). On the other hand, the results are extremely sensitive to the choice of the electron-water pseudopotential. Most previous studies of electron solvation in water represent the electron-water pseudopotential as a sum of two-body interactions. Studies of electron hydration and hydrated-electron spectroscopy show that the potentials developed for this purpose (145) could account semiquantitatively for the general features of electron-solvation structure and energetics in water and water clusters. Taking into account the many-body aspects of the electronic polarizability contributions to the electron-water pseudopotential (149) has led to improved energy values that were typically different by 10%–20% from the original results. In contrast, including these many-body interactions in the tunneling calculation is found to make a profound effect (see below), an increase of $\sim$2 orders of magnitudes in the transmission probability of electron through water in the deep tunneling regime. There are two reasons for this. First, as already noted, tunneling processes are fast relative to characteristic nuclear relaxation times. The latter is disregarded, leaving the electronic polarizability as the only solvent response in the present treatment. Second, variations of the interaction potentials enter exponentially into the tunneling probability, making their effects far larger than the corresponding effect on solvation. It should be kept in mind that including the solvent electronic polarizability in simulations of quantum mechanical processes in solution raises some conceptual difficulties. The simulation results described below are based on the approach to this

problem described elsewhere (133, 135). In what follows, model *B* refers to the the corrected electron-water pseudopotential used in these papers whereas model *A* refers to the original pseudopotential of Barnett et al (145) [see the original publications 133–137 for details of the water-water and water-metal potentials used in these calculations].

The results described below illustrate the principal factors affecting the transmission process: (*a*) the dimensionality of the process, (*b*) the effect of layer structure and order, (*c*) the effect of resonances in the barrier, and (*d*) the signature of band motion. The simulations consist of first preparing water layer structures on (or between) the desired substrates using classical MD simulations, then setting the Schrödinger equation for the electron-transmission problem on a suitable grid, and finally, computing the transmission probabilities.

Figure 8 shows the results of such calculations for the transmission probability as a function of the incident electron energy. The results for the polarizable model (*B*) are seen to be in remarkable agreement with the expectation based on the lowering of the effective rectangular barrier by 1.2 eV, whereas those obtained using model *A*, which does not take into account the many-body nature of the interaction associated with the water electronic polarizability, strongly underestimates the transmission probability. In fact, model *A* predicts the transmission probability in water to be lower than in a vacuum, in qualitative contrast to our observations.

Next, consider the effect of orientational ordering of water dipoles on the metal walls. Water adsorbs with its oxygen on the metal surface and the hydrogen atoms pointing away from it, leading to net surface dipole density directed away from the wall. Simulations yield $\sim 5 \cdot 10^{-11}$ Coulomb/m for this density. (I. Benjamin, A. Nitzan, unpublished data). This is an important factor in the reduction of the surface-work function of many metals due to water adsorption (132, 150). The sparse-dotted line in Figure 8 shows the transmission probability for a model obtained from model *A* by eliminating the attractive oxygen/metal-wall interaction, thereby destroying the preferred orientational ordering at the water-metal interface. We see that the existence of a surface dipole in the direction that reduces the work function is associated with a larger transmission probability, as expected.

Traditional approaches to electron transfer are based on a continuum dielectric picture of the solvent, where the issue of the tunneling path rarely arises. Barring other considerations, the exponential dependence of tunneling probabilities on the path length suggests that the tunneling process will be dominated by the shortest possible, i.e. one-dimensional, route. A closer look reveals that electron tunneling through water is inherently three-dimensional (e.g. see 133, Figure 7). An interesting demonstration of the importance of the three-dimensional structure of the water layer in determining the outcome of the tunneling process was given in Benjamin et al (136), where the transmission probability was computed, using the configuration of Figure 8 and model *B* at room temperature, for water configurations prepared in the presence of a strong electric field pointing along the tunneling (x) axis. In such layers, the water dipoles point on the average along this axis. The

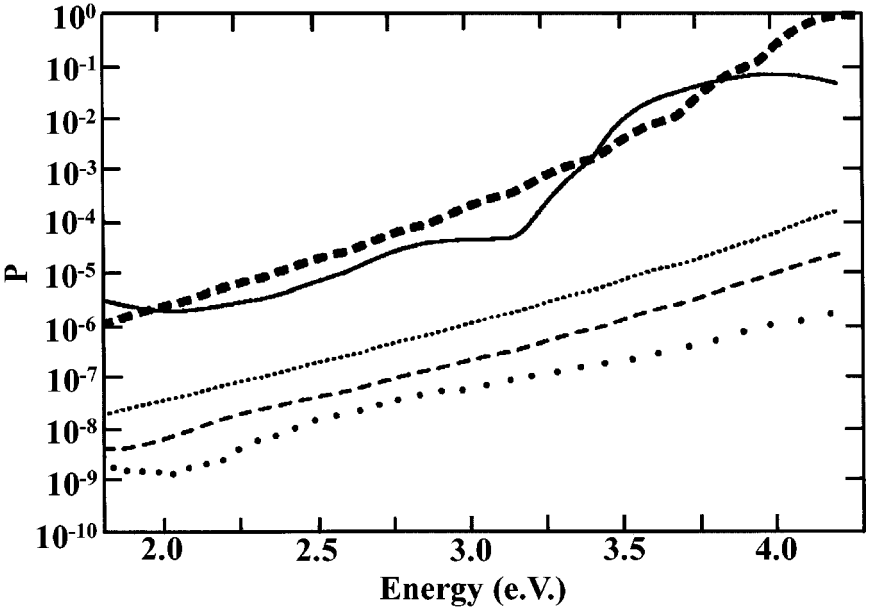

Figure 8 Electron transmission probability as a function of the incident energy. Shown are one-to-all transmission results with the electron incident in the direction normal to the water layer. These results are averaged over six equilibrium water configurations sampled from an equilibrium trajectory for the water system. This system contains 192 water molecules confined between two walls separated by 10 Å, with periodic boundary conditions, with period 23.5 Å in the directions parallel to the walls, at 300 K. These data correspond to three water monolayers between the walls. *Thin dashed line*: Results from model A (see text). *Full line*: Results from model *B*. Also shown are the corresponding results for tunneling through a vacuum, i.e. through a bare rectangular potential barrier of height 5 eV (*thick-dotted line*), and through a similar barrier of height 3.8 eV (*thick-dashed line*), which corresponds to the expected lowering of the effective barrier for tunneling through water. The *thin-dotted line* is the transmission probability computed for model *A* modified by eliminating the attractive part of the water-metal interaction, thereby eliminating the preferred orientational ordering of the water dipoles at the water-metal interface. (Reproduced from Reference 135 and used by permission.).

electric field was removed during the subsequent tunneling calculation. The computed one-to-all transmission for electrons incident in the *x* direction shows several orders of magnitude difference between the probabilities calculated for electron incident in the direction of the induced polarization and against this direction. Microscopic reversibility implies that the corresponding one-dimensional process should not depend on the tunneling direction, positive or negative, along the *x* axis. The observed behavior is therefore associated with the three-dimensional nature of the process. It shows that the angular distribution associated with the transmission through such layers depends strongly on the transmission direction and suggests

that asymmetry in current-voltage dependence of transmission current should exist beyond the linear regime.

Next consider the possibility of resonance-assisted tunneling. Such resonances are found (138) in a range of ~1 eV below the 5 eV vacuum barrier, and their existence correlates with the observation of weakly bound states of an electron in neutral configurations of bulk water. Mosyak et al (135) have found that such states appear in neutral water configurations in both models *A* and *B*; however, only model *B* shows such states at negative energies. Moreover, these states are considerably more extended in systems described by model *B* compared with the corresponding states of model *A* (135). The possible effect of bound electron states in water on electron-transmission probability through water was raised in the past (151). Peskin et al (138) have recently identified the source of the resonances seen in our simulations as transient vacancies in the water structure. We emphasize again that because these results were obtained for static water configurations, their actual role in electron transmission through water is yet to be clarified.

The effective barrier to electron tunneling in water has been the subject of many discussions in the STM literature (22, 128, 131, 152). Although the absolute numbers obtained vary considerably depending on the systems studied and on experimental setups and conditions, three observations can be made. (*a*) Tunneling is observed at large tip-surface distances, sometimes exceeding 20 Å (22, 131, 152). (*b*) The barrier, estimated using a one-dimensional model from the distance dependence of the observed current, is unusually low, of the order of 1 eV in systems involving metals with work functions of 4–5 eV. (*c*) The numbers obtained scatter strongly: The estimated barrier height may be stated to be 1 ± 1 eV. (*d*) The apparent barrier height appears to depend on the polarity of the bias potential.

It should be kept in mind that even in a vacuum STM, the barrier to tunneling is expected to be lower than the work functions of the metals involved because of image effects associated with the fast electronic response of the electrodes (29). Nevertheless, the reduction of barrier height in the aqueous phase seems to be considerably larger. Taking the vacuum barrier as input in our discussion, let us consider the possible roles of the solvent. These can arise from the following factors: (*a*) the position, on the energy scale, of the "conduction band" of the pure solvent (by "conduction band" we mean extended electronic states of an excess electron in the neutral solvent configuration); (*b*) the effect of the solvent on the electrode workfunction; (*c*) the hard cores of the atomic constituents (in the present case the water oxygens, which make a substantial part of the physical space between the electrodes inaccessible to the electron); and (*d*) the possibility that the tunneling is assisted by resonance states supported by the solvent. Such resonances can be associated with available molecular orbitals—this does not appear to be the case in water—or with particular transient structures in the solvent configurations, as discussed above.

Factors *b–d* are usually disregarded in theories of electron transfer, whereas a common practice is to account for the first factor by setting the potential barrier height at a value, below the vacuum level, determined by the contribution of the solvent electronic polarizability. This value can be estimated as the Born energy of

a point charge in a cavity of intermolecular dimensions, say a radius of ∼5 au, in a continuum with the proper dielectric constant, here the optical dielectric constant of water, $\varepsilon_\infty = 1.88$. This yields $e^2(2a)^{-1}[\varepsilon_\infty{}^{-1} - 1] \sim -1.3$ eV, the same order as the result of a more rigorous calculation by Schmickler & Henderson (153) and in agreement with experimental results on photoemission into water (132). It should be noted that this number was obtained for an infinite bulk of water and should be regarded as an upper limit for the present problem.

The simulations described above shed some light on the roles played by the other factors listed above. First, we find that lowering the metal work function by the orientational ordering of water dipoles at the metal surface does affect the tunneling probability, as discussed above and shown in Figure 8. Second, the occupation of much of the physical space between the electrodes by the impenetrable oxygen cores strongly reduces the tunneling probability. In fact, if these two factors exist alone, the computed tunneling probability is found to be considerably lower than in the corresponding vacuum process (see 133, Figure 7). Even including the effect of the water electronic polarizability (i.e. attractive r^{-4} terms) in the two-body electron-water pseudopotential (model *A*), it is not sufficient to reverse this trend, as seen in Figure 8. Taking into account the full many-body nature of this interaction is found to be essential for obtaining the correct qualitative effect of water, i.e. barrier lowering relative to vacuum.

The estimate of the magnitude of this lowering effect in our simulations can be done in two ways. One is to fit the absolute magnitude of the computed transmission probability to the result obtained from a one-dimensional rectangular barrier of width given by the distance *s* between the electrodes (134). This is done in Figure 9 for systems with 1–4 monolayers of water ($s = 3.6, 6.6, 10.0, 13.3$ Å).[15] The following points should be noted:

(1) The effective barrier to tunneling computed with the fully polarizable model *B* is reduced by at least 0.5 eV (from the bare value of 5 eV used in these simulations) once a bulk has been developed in the water layer, i.e. once the number of monolayers is larger than two.

(2) The equivalent calculation done with model *A*, in which water polarizability is accounted for only on the two-body level, yields an effective barrier higher than the vacuum barrier.

(3) For the very thin layers studied, the effective barrier height depends on the layer thickness. This behavior [which supports a recent experimental observation by Nagy (130)] is expected to saturate once a well-defined bulk is developed.

Following common practice in STM studies, another way to discuss the effective simulated barrier is to fit the distance dependence of the observed tunneling

[15]It should be emphasized that these results were not statistically averaged over many water configurations, so the absolute numbers obtained should be taken only as examples of a general qualitative behavior.

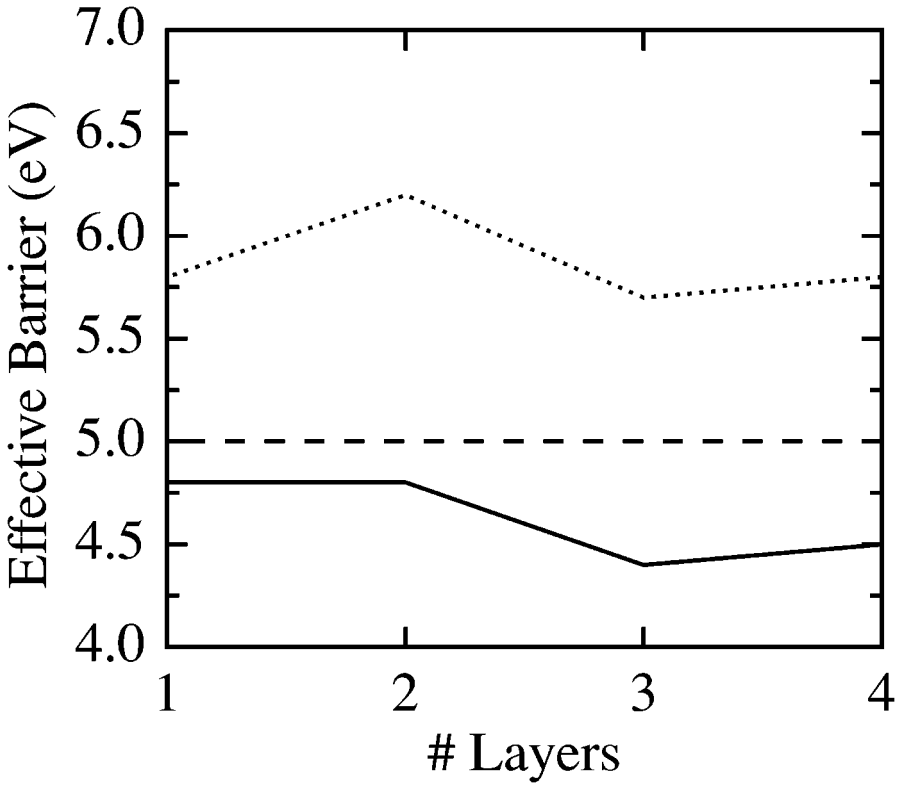

Figure 9 Effective one-dimensional barrier height for electron transmission through water, displayed as a function of number of water layers. *Solid, dotted,* and *dashed lines* correspond to models *A* and *B,* and to the bare (5 eV) barrier, respectively. See text for details. (Reproduced from Reference 134 and used by permission.)

probability to the analytical result for a rectangular barrier. This practice can yield very low apparent barriers in cases where tunneling is influenced by resonance structures (137). Moreover, since the existence and energies of these resonances in water depend on local structures that evolve over time, it is possible that the characteristic scatter of data that appears in these measurements (22, 128, 131, 152) may arise not only because of experimental difficulties but also from intrinsic system properties.

The existence in water of transient structures that support excess electron resonances and the possible implications of these resonances in enhancing the tunneling probability, and the apparent barrier height, raises again the issue of timescales. In particular, the lifetimes of these resonance states is of considerable interest, since they determine the duration of the electron capture by the water film and, as a consequence, the possibility that water dynamics and thermal relaxation become important on this timescale. Peskin et al (138) have determined these lifetimes

by a direct evaluation of the complex eigenvalues associated with the corresponding resonance structures, using a filter diagonalization method with the imaginary boundary-conditions Hamiltonian. The resulting eigenvalues have imaginary parts of the order ~0.05 eV, implying lifetimes of the order ≤10 fs. An alternative way to probe the dynamics of electron tunneling in water is by evaluating the corresponding traversal times (see Section 3.1). Here the timescale for possible interaction between the excess electron and barrier motions can be determined both near and away from resonance energies. Galperin et al (94) have applied the internal clock approach of Section 3.1 to this problem, starting from the one-to-all transmission probability, shown in Equation 63, written in the form

$$\sigma = \frac{1}{\pi}\langle\phi_{in}(E)|\hat{\varepsilon}_{in}^{*}\hat{G}^{\dagger}\hat{\varepsilon}_{out}\hat{G}\hat{\varepsilon}_{in}|\phi_{in}(E)\rangle, \qquad 125.$$

where $\phi_{\rm in}$ denotes an incoming state in the reactant region and $\varepsilon_{\rm in}$ and $\varepsilon_{\rm out}$ are the absorbing boundary functions in the reactant (incoming) and product (outgoing) regions, respectively. In the present application, the electron is taken to have two internal states, so that if x is the tunneling direction, $\phi_{in} = \left(e^{ikx}/\sqrt{v}\right)\binom{1}{0}$. The Green's operator is given by $\hat{G} = (E - \hat{H}_0 + i(\hat{\varepsilon}_{in} + \hat{\varepsilon}_{out}))^{-1}$ with $\hat{H}_0$ replaced by

$$\hat{H} = \hat{H}_0\begin{pmatrix}1 & 0\\ 0 & 1\end{pmatrix} + \lambda\hat{F}(x)\begin{pmatrix}0 & 1\\ 1 & 0\end{pmatrix}, \qquad 126.$$

where λ is a constant and where $F(x) = 1$ in the barrier region and 0 outside it. The approximate scattering wavefunction,

$$|\psi(E)\rangle = i\hat{G}(E)\hat{\varepsilon}_{in}|\phi_{in}(E)\rangle = \begin{pmatrix}\psi_1(E)\\ \psi_2(E)\end{pmatrix}, \qquad 127.$$

is evaluated using iterative inversion methods (148). The transmission probabilities into the $|1\rangle$ and $|2\rangle$ states are obtained from

$$\mathcal{T}_i(E) = \langle\psi_i(E)|\hat{\varepsilon}_{out}|\psi_i(E)\rangle; \quad i = 1, 2. \qquad 128.$$

$\mathcal{T}_i$ are equivalent to $|c_i|^2$, where $c_i (i = 1, 2)$ are defined above in Equation 73. Accordingly,

$$\tau(E) = \lim_{\lambda\to 0}\left(\frac{\hbar}{|\lambda|}\sqrt{\frac{\mathcal{T}_2(E)}{\mathcal{T}_1(E)}}\right). \qquad 129.$$

Figures 10 and 11 (94) display some results of this calculation. Figure 10 shows calculated traversal times as functions of incident electron energy for an electron transmitted through a layer of three water films between two platinum electrodes (the distance between the electrodes is $d = 18.9$ au. Shown is τ/τ_0 for several configurations of this system, where τ_0 is the tunneling time associated with the bare vacuum barrier (same geometry with no water). The transient nature of the water structures that give rise to the resonance features is seen here. Note that the difference between different configurations practically disappears

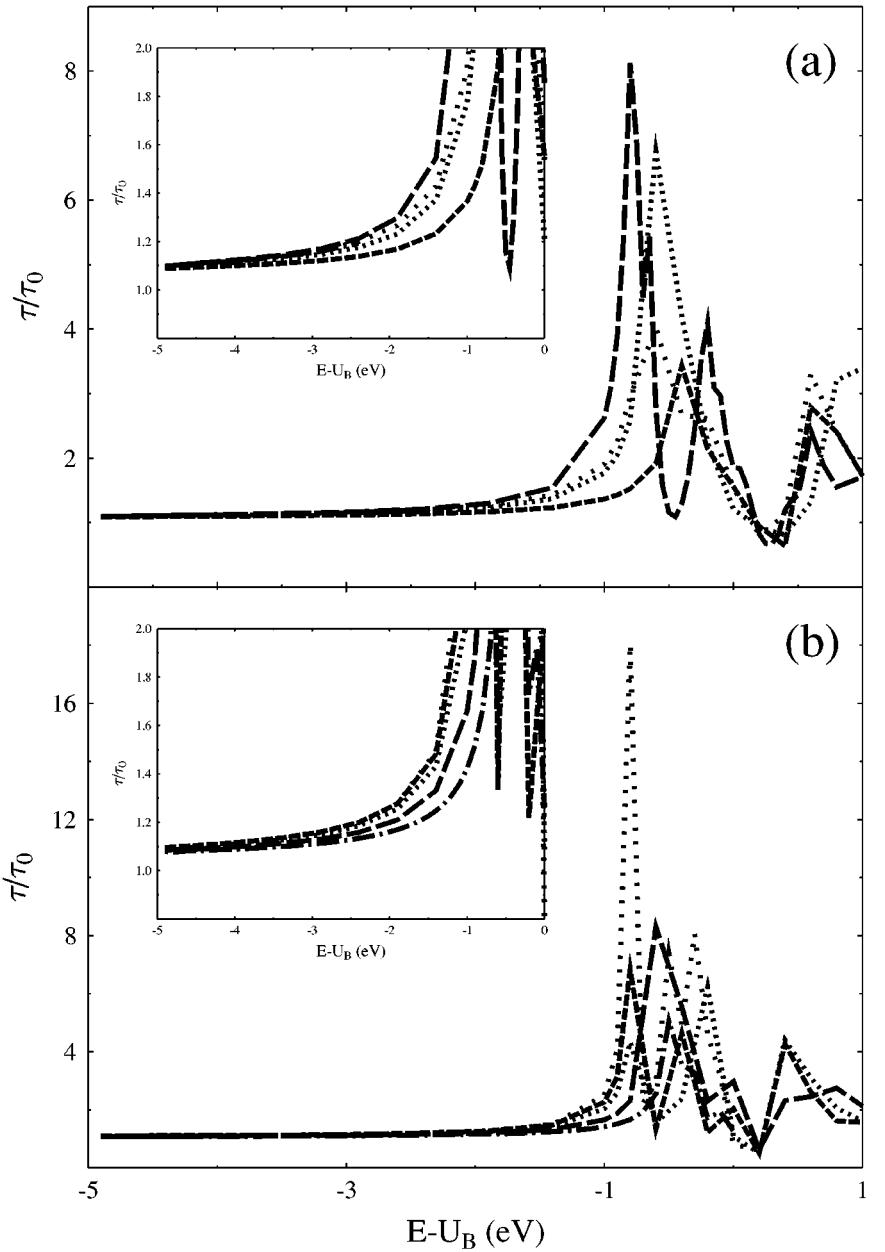

Figure 10 The ratio τ/τ_0 (see text) computed for different static configurations of (*a*) three and (*b*) four monolayer water films, displayed against the incident electron energy. The *inset* shows an enlarged vertical scale for the deep tunneling regime. (Reproduced from Reference 94 and used by permission.)

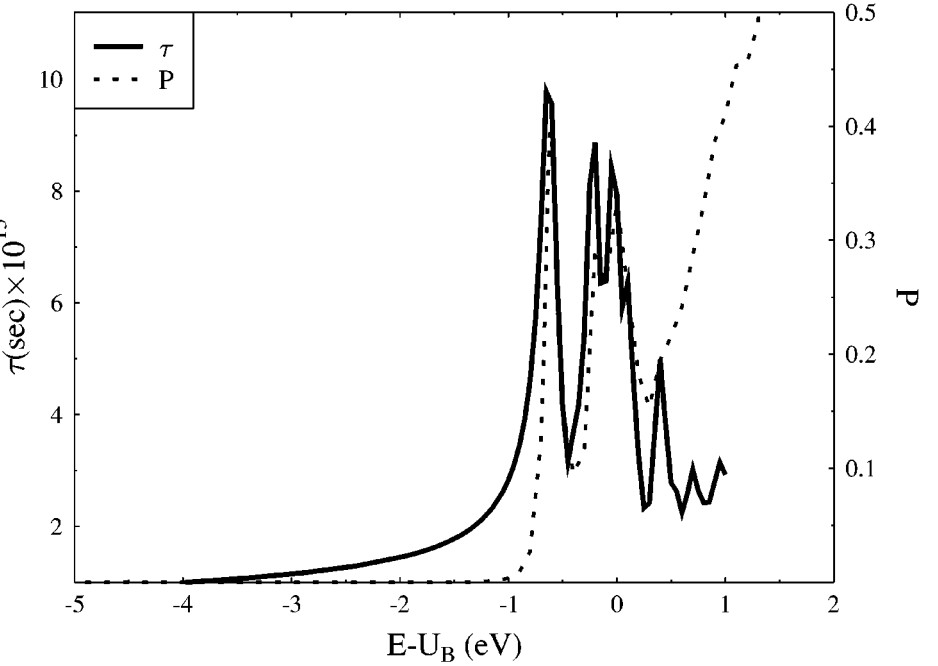

Figure 11 The tunneling traversal time (*full line*; *left vertical scale*) and the transmission probability (*dotted line*; *right vertical scale*) computed as functions of incident electron energy for one static configuration of the 3-monolayer water film. (Reproduced from Reference 94 and used by permission.)

for energies sufficiently below the resonance regime, where the ratio between the time computed in the water system and in the bare barrier is practically constant, approximately 1.1. Figure 11 shows, for one of these configurations, the tunneling time and the transmission probability, both as functions of the incident electron energy. We see that the energy dependence of the tunneling time follows this resonance structure closely. In fact, the times (3–15 fs) obtained from the peaks in Figures 10 are consistent with the resonance lifetimes estimated in Peskin et al.

We conclude this discussion with two more comments. First, in the above analysis, the possibility of transient "contamination" of the tunneling medium by foreign ions has been disregarded. Such ions exist in most systems used in underwater STM studies, and the appearance of even one such ion in the space of 10–20 Å between the electrodes can have a profound effect on the tunneling current behavior. This may add another source of scatter in the experimental results. Second, as discussed, changes in the water structure between the electrodes may appear also as bias-dependent systematic effects. Thus, the asymmetry in the bias dependence of the barrier height observed in Pan et al (128), Hahn et al (22),

and Hong et al (131) may be related to the asymmetric transmission properties of orientationally ordered layers.

5. OVERBARRIER TRANSMISSION

Our discussion so far has focused on electron-transmission processes that at zero-temperature can take place only by tunneling. This section provides a brief overview of transmission processes where an electron incident on a molecular barrier carries a positive (above-ground–state vacuum) energy. It should be emphasized that this in itself does not mean that transmission can take place classically. If the incident energy is in the band gap of the molecular spacer, zero-temperature transmission is still a tunneling process. Still, this type of phenomenon is distinct from those discussed in the other parts of this review, for several reasons. First, positive-energy transmission (and reflection), essentially scattering processes, are amenable to initial-state control and to final-state resolution that are not possible in negative-energy processes. Second, a positive-energy electron interacts with a large density of medium states; therefore, the probability for resonance or near resonance transfer is considerably larger, implying also a larger cross-section for dephasing and inelastic energy loss. Third, at this range of energies, conventional quantum-chemistry approaches as well as pseudopotentials derived from low-energy electronic-structure data can be very inaccurate. Finally, at high enough energies, electronic excitations and secondary electron generation become important factors in the transmission mechanism. For the last two reasons the numerical approaches described in Section 2.6–8 are not immediately applicable.

The effect of adsorbates on photoelectrons emitted from surfaces has been studied for almost a century (154, 155). These experiments were partially motivated by their practical ramifications whereby the surface work function was modified by the adsorbate (156). Recently, the development of tunable ultraviolet light sources has enabled studies of energy-resolved photoelectron spectroscopy. This eventually led to studies of photoelectron energy distribution for photoelectrons produced from metal surfaces covered with self-assembled monolayers of organic molecules, or organized organic thin films (147, 157–162). These films are prepared either with the Langmuir-Blodgett technique (163) or by self-assembly from vapor or solution. One of the earlier experiments of this kind was the measurement of transmitted electron energy distribution for photoelectrons produced from a Pt (111, 111a) surface covered with several layers of water (139). The transmission probability decreased exponentially with increasing numbers of water layers; however, this number does not affect the energy distribution of the emitted electrons, indicating that transmission in this system is independent of the electron energy and that inelastic energy loss is small. These results should, however, be regarded with caution in view of LEET data (142) that indicate that energy loss from a transmitted electron to water nuclear motion may be quite efficient. The latter observation is supported by estimates (143) of the distance (20–50 Å) traversed by electrons

photoejected into water at subexcitation energies before their capture to form the precursor of solvated electrons.

Unlike water, the electron affinity $A = -V_0$ of hydrorcarbon layers is negative, i.e. their LUMOs, or in the language of solid state physics, the bottom of their electron-condition band is above vacuum energy [$V_0 = 0.8$ eV for bulk hydrocarbons (164)]. Indeed, a threshold for electron photoemission from silver, covered with a monolayer of cadmium stearate $[CH_3(CH_2)_{16}COO^-]_2Cd^{2+}$, or arachdic acid $CH_3(CH_2)_{16}COOH$, is observed (159). Above 0.8 eV, photoemission from these surfaces proceeds with efficiency close to one, turning down again at higher energies. Oscillations in the transmission probability through similar films as a function of the initial electron energy were interpreted in terms of the electronic-band structure of the film (147). This interpretation gains further support from the observation of the large sensitivity of the transmission probability to the film structure in the lateral dimension (161), and from the strong effect of film ordering (161). This does not exclude what is often taken to express a single molecule effect—a strong preference of the phtoemission to be directed along the axis of the molecular adsorbate (158). Finally, using chiral molecular self-assembled monolayers (L or D polyalanine polypeptides) has revealed that electron transmission of spin-polarized electrons depends, with a high degree of selectivity, on the chirality of the layer (162).

Another way to study electron interactions with molecular layers is to send an electron beam from the vacuum side onto a molecular film condensed on a suitable, usually metallic, substrate. In LEET spectroscopy developed by Sanche and coworkers (141), the electron-transmission spectrum is measured by monitoring the current arriving at the metal substrate as a function of the incident electron energy and direction. Similarly, the reflected electron beam can be analyzed with respect to energy and angular distribution, yielding electron-diffraction data, energy-loss spectra, and energy-loss excitation spectra. The same experimental setup can be used to study the effect of electron trapping, electron-stimulated desorption, and electron-induced chemical reactions on the molecular films. [For a recent review of these types of studies and references to earlier work, see Sanche (141).] Here we focus on observations from LEET experiments that are relevant to our present subject. First, the prominence of the elastic and quasielastic component of the transmitted intensity, observed in most experiments of this kind, is in agreement with the photoemission experiments discussed above. Second, a threshold of a few tens of electron volts (relative to the vacuum level) is seen for transmission through alkane and rare gas layers, indicating negative electron affinities of these layers and providing an estimate for the position of the bottom of the layers' conduction bands. Third, conduction peaks below this threshold are attributed to tunneling assisted by local states inside the gap (125). This is the analog of the bridge-assisted tunneling discussed in Section 2, except that the film constitues a three-dimensional barrier in which the local states are distributed randomly in position and energy. As discussed in Section 3.4, thermal relaxation and dephasing processes manifest themselves in a characteristic thickness dependence of the transmission probability as the processes change from tunneling to hopping dominated with increasing barrier

width (see Figure 7). Fourth, the electron transmission spectra closely reflects the band structure of the corresponding layer. This should not be taken as evidence for ballistic transport, in fact this observation holds only for the inelastic components of the emission intensity. Rather, the electron propagation through the molecular environment is viewed as a sequence of scattering events, with cross-sections that are proportional to the density of available states (165). The resulting averaged-mean free path is therefore inversely proportional to the density of states at an energy that (as long as the absolute energy loss is small) may be approximated by the incident energy. Finally, the transmission can be strongly affected by resonances, i.e. negative ion formation. This in turn may greatly increase the probability for inelastic energy loss (141). These processes are observed in the high-resolution electron energy-loss spectroscopy, by monitoring the energy of reflected electrons, but they undoubtedly play an equally important part in the transmission process.

As already mentioned, while the theoretical methods discussed in previous sections of this review are general, their applicability to electron transmission in the positive energy regime needs special work because standard quantum-chemistry calculations usually address negative energy regimes and bound electronic states, and because pseudopotentials are usually derived from fitting results of such ab initio calculations to analytical forms based on physical insight. Model calculations that demonstrate some of the concepts discussed above are shown in Figures 12 and 13 (147). Figure 12 compares the transmission probability ("one to all," with the incident electron perpendicular to the barrier) through a one-dimensional rectangular barrier of height 3 eV and width 1.2 nm as a function of the incident electron energy measured relative to the barrier top with the transmission through a three-dimensional slab of four Ar layers cut out of an Ar crystal in the {100} direction. The latter results are obtained with a spatial-grid technique using the electron-Ar pseudopotential of Space et al. (166). The oscillations of the dotted line in Figure 12 are interference patterns associated with the finite width of the layers. The full line in Figure 12 also shows such oscillations, but in addition, a prominent dip above 4 eV corresponds to a conduction band gap of this thin-ordered layer. The transmission through the disordered layer (dashed line) is considerably less structured (smoother shapes should be obtained with more configurational averaging); in particular, the dip associated with the bandgap has largely disappeared. Figure 13 compares the transmission (one-to-all) versus electron energy for an electron incident in the normal direction on ordered Ar films made of 2, 4, and 6 atomic monolayers (prepared by cutting them off an Ar crystal, as described above). Already at six-layer thickness, the observed transmission dip is very close to its bulk value, indicating that the band structure is already well developed.

These calculations investigate transmission through static nuclear structures and consequently cannot account for thermal relaxation and dephasing effects. In the other extreme limit one uses stochastic models (167) that become accurate when the molecule film is thick enough so that the electron goes through multiple scattering events before being transmitted through or reflected from the film. Such an approach has been used (141, 168) to describe the energy distributions of

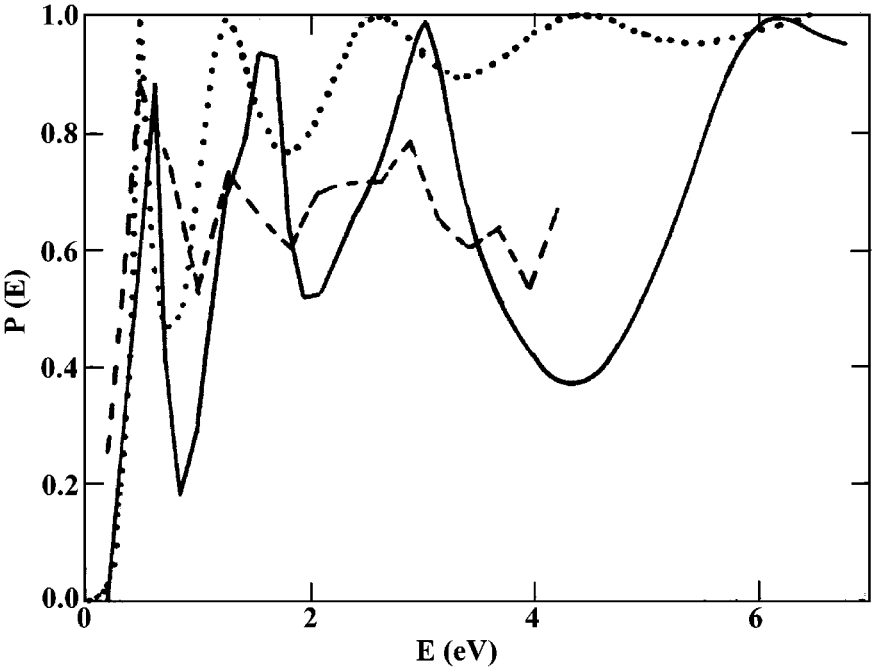

Figure 12 *Dotted line*: Transmission probability through one-dimensional rectangular barrier characterized by height of 3 eV and width of 12 Å, as a function of incident electron energy measured relative to the barrier top. *Full line*: Electron transmission through a slab made of four Ar layers, cut out of an FCC Ar crystal in the {100} direction. *Dashed line*: Same results obtained for a disordered Ar slab, obtained from the crystalline layer by a numerical thermal annealing at 400 K next to an adsorbing wall using molecular dynamics propagation. The results shown are averaged over four such disordered Ar configurations (see 147 for more details). (Reproduced from Reference 147 and used by permission.)

electrons reflected from molecular films and their relation to the density of excess electron states in the film.

6. CONCLUSIONS AND OUTLOOK

This review has described the current status of theoretical approaches to electron transmission and conduction in molecular junctions. In particular, Section 2 constitutes an account of theoretical approaches to this problem for static junctions, whereas Section 3 discusses approaches that focus on dephasing and thermal relaxation effects. It is important to note that even though our methodology follows a stationary, steady state viewpoint of all processes studied, the issue of relative timescales of different processes has played a central role in our analysis.

Current studies of molecular junctions focus on general methodologies on the one hand and on detailed studies of specific systems on the other. We have described

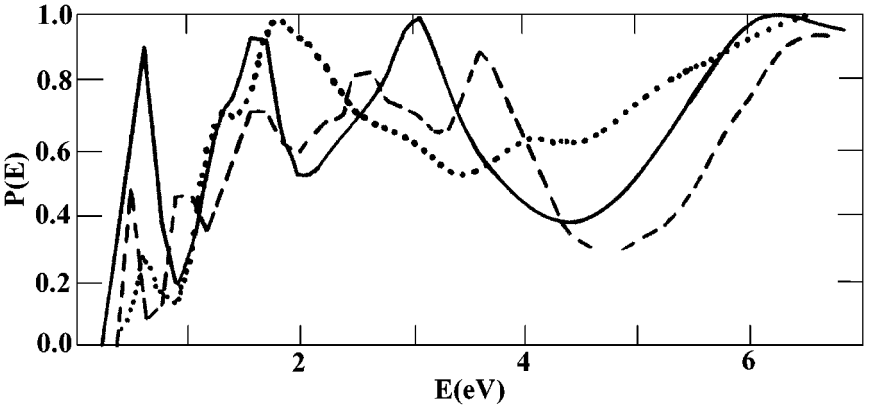

Figure 13 The computed transmission probabilities, vs electron energy, for an electron incident on slabs cut out of an FCC Ar crystal in the {100} direction. Shown are transmission probabilities vs incident electron energy through slabs made of two monolayers (*dotted line*), four monolayers (*full line*), and six monolayers (*dashed line*). (Reproduced from Reference 147 and used by permission.)

in detail recent computations of electron transmission through water layers and have described other studies on prototypes of molecular wires. Two imporant classes of molecular wires have now become subjects of intense research, even development effort. These are DNA wires and carbon nanotubes. Although the general principles discussed in this review apply also to these systems, the scope of recent research on special structure-function properties of these wires merits a separate review.

Returning to theoretical issues, we have outlined some open problems in the methodology of treating these many-body, strongly interacting, nonequilibrium open systems. One additional direction not covered is the possibility of controlling the operation of such junctions using external forces (as opposed to control of function by varying the structure). Several recent studies point out the possibility of controlling transport processes by external fields (169). The specific and selective nature of molecular optical response make molecular junctions strong potential candidates for such applications.

In conclusion, electron transmission and conduction processes in small molecular junctions combine the phenomenology of molecular electron transfer with structural problems associated with design and construction of such junctions, and with the need to understand their macroscopic transport properties. In addition, the potential technological promise suggests that research in this area will intensify.

ACKNOWLEDGMENTS

This work was supported by the US-Israel Binational Science Foundation. I am indebted to many colleagues with whom I have collaborated and/or discussed various aspects of this work: I Benjamin, M Bixon, A Burin, B Davis, D Evans,

M Galperin, P Hänggi, J Jortner, R Kosloff, A Mosyak, V Mujica, R Naaman, U Peskin, E Pollak, M Ratner, D Segal, T Seideman, D Tannor, MR Wasielewski, J Wilkie, and S Yaliraki. I also thank S Datta and L Sanche for allowing me to use figures from their work.

LITERATURE CITED

1. Jortner J, Bixon M, eds. 1999. *Advances in Chemical Physics: Electron Transfer—From Isolated Molecules to Biomolecules*, Vol. 106. New York:Wiley
2. Schmickler F. 1996. *Interfacial Electrochemistry*. Oxford, UK: Oxford Univ. Press
3. Joachim C, Roth S, eds. 1997. *Atomic and Molecular Wires*, Vol. 341. Dordrecht: Kluwer
4. Jortner J, Ratner M, eds. 1997. *Molecular Electronics*. Oxford, UK: Blackwell Sci.
5. Marcus RA. 1965. *J. Chem. Phys.* 43:679
6. Gosavi S, Marcus RA. 2000. *J. Phys. Chem.* 104:2067–72
7. Tour JM. 1996. *Chem. Rev.* 96:537
8. Sachs SB, Dudek SP, Sita LR, Newton JF, Feldberg SW, Chidsey CED. 1997. *J. Am. Chem. Soc.* 119:10563
9. Isied SS, Ogawa MY, Wishart JF. 1992. *Chem. Rev.* 92:381
10. Mutz MW, Case MA, Wishart JF, Ghadiri MR, McLendon GL. 1999. *J. Am. Chem. Soc.* 121:858–59
11. Holmlin RE, Dandliker PJ, Barton JK. 1997. *Angew. Chem. Int. Ed. Engl.* 36:2714
12. Lewis FD, Wu TF, Zhang YF, Letsinger RL, Greenfield SR, Wasielewski MR. 1997. *Science* 277:673–76
13. Meggers E, Michel-Beyerle ME, Giese B. 1998. *J. Am. Chem. Soc.* 120:12950–55
14. Ghiggino KP, Clayton AHA, Lawson JM, Paddon-Row MN. 1996. *N. J. Chem.* 20:853
15. Guo HL, Facci JS, Mclendon G. 1995. *J. Phys. Chem.* 99:8458
16. Langlais VJ, Schlittler RR, Tang H, Gourdon A, Joachim C, Gimzewski JK. 1999. *Phys. Rev. Lett.* 83:2809–12
17. Roth S, Burghard M, Fischer CM. 1997. See Ref. 4, pp. 255–80
18. Dhirani A, Lin PH, Guyot-Sionnest P. 1997. *J. Chem. Phys.* 106:5249–53
19. Reed MA, Zhou C, Muller CJ, Burgin TP, Tour JM. 1997. *Science* 278:252–54
20. Datta S, Tian WD, Hong SH, Reifenberger R, Henderson JI, Kubiak CP. 1997. *Phys. Rev. Lett.* 79:2530–33
21. Tian WD, Datta S, Hong SH, Reifenberger R, Henderson JI, Kubiak CP. 1998. *J. Chem. Phys.* 109:2874–82
22. Hahn JR, Hong YA, Kang H. 1998. *Appl. Phys. A* 66:S467–72
23. Zhou C, Muller CJ, Reed MA, Burgin TP, Tour JM. 1997. See Ref. 4, pp. 191–213
24. Porter JD, Zinn AS. 1993. *J. Phys. Chem.* 97:1190–203
25. Slowinski K, Slowinska KU, Majda M. 1999. *J. Phys. Chem.* 103:8544–51
26. McConnel HM. 1961. *J. Chem. Phys.* 35:508–15
27. Onipko A, Klymenko Y. 1998. *J. Phys. Chem. A* 102:4246–55
28. Simmons JG. 1963. *J. Appl. Phys.* 34:1793–803
29. Lang ND. 1988. *Phys. Rev. B* 37:10395
30. Tersoff J, Hamman DR. 1985. *Phys. Rev. B* 5031:805
31. Bardeen J. 1961. *Phys. Rev. Lett.* 6:57
32. Landauer R. 1970. *Philos. Mag.* 21:863–67
33. Imry Y. 1997. *Introduction to Mesoscopic Physics*. Oxford, UK: Oxford Univ. Press
34. Miller WH. 1975. *J. Chem. Phys.* 62:1899–906
35. Miller WH, Schwartz SD, Tromp JW. 1983. *J. Chem. Phys.* 79:4889–98

36. Galperin M, Segal D, Nitzan A. 1999. *J. Chem. Phys.* 111:1569–79
37. Mujica V, Kemp M, Ratner MA. 1994. *J. Chem. Phys.* 101:6849–64
38. Newns DM. 1969. *Phys. Rev.* 178:1123
39. de Andrade PCP, Onuchic JN. 1998. *J. Chem. Phys.* 108:4292–98
40. Nitzan A. 2001. *J. Phys. Chem.* In press
41. Magoga M, Joachim C. 1997. *Phys. Rev. B* 56:4722–9

41a. Magoga M, Joachim C. 1997. *Phys. Rev. B* 57:1820–23

41b. Magoga M, Joachim C. 1997. *Phys. Rev. B* 59:16011–21

42. Yaliraki SN, Kemp M, Ratner MA. 1999. *J. Am. Chem. Soc.* 121:3428–34
43. Biscarini F, Bustamante C, Kenkre VM. 1995. *Phys. Rev. B* 51:11089–101
44. Emberly EG, Kirczenow G. 1999. *Phys. Rev. B* 60:6028–33
45. Hall LE, Reimers JR, Hush NS, Silverbrook K. 2000. *J. Chem. Phys.* 112:1510–21
46. Faglioni F, Claypool CL, Lewis NS, Goddard WA. 1997. *J. Phys. Chem.* 101:5996–6020
47. Larsson S, Klimkans A. 1999. *Theochem. J. Mol. Struct.* 464:59–65
48. Yaliraki SN, Roitberg AE, Gonzalez C, Mujica V, Ratner MA. 1999. *J. Chem. Phys.* 111:6997–7002
49. Newton MD. 1991. *Chem. Rev.* 91:767
50. Emberly EG, Kirczenow G. 1999. *J. Phys. C* 11:6911–26
51. Koopmans T. 1933. *Physica* 1:104
52. Kergueris C, Bourgoin JP, Palacin S, Esteve D, Urbina C, et al. 1999. *Phys. Rev. B* 59:12505–13
53. Miskovic ZI, English RA, Davison SG, Goodman FO. 1997. *J. Phys. Conduct. Matter* 9:10749–60
54. Seideman T, Miller WH. 1992. *J. Chem. Phys.* 96:4412

54a. Seideman T, Miller WH. 1992. *J. Chem. Phys.* 97:2499

55. Liebsch A. 1997. *Electronic Excitations at Metal Surfaces*, pp. 5–48. New York: Plenum

55a. Liebsch A. 1997. See Ref. 55, pp. 283–308

56. Lang ND. 1995. *Phys. Rev. B* 52:5335–42
57. Lang ND, Avouris P. 2000. *Phys. Rev. Lett.* 84:358–61
58. Parr RG, Yang W. 1989. Density Functional Theory of Atoms and Molecules *Density Functional Theory of Atoms and Molecules*. Oxford, UK: Oxford Univ. Press
59. Di Ventra M, Pantelides ST, Lang ND. 2000. *Phys. Rev. Lett.* 84:979–82
60. Hirose K, Tsukada M. 1995. *Phys. Rev. B* 51:5278–90
61. Mujica V, Roitberg AE, Ratner MA. 2000. *J. Chem. Phys.* 112:6834–39
62. Szabo A, Ostlund NS. 1989. *Modern Quantum Chemistry: Introduction to Advanced Electronic Structure Theory*. New York: McGraw-Hill
63. Burke H, Gross EKU. 1998. In *Density Functionals: Theory and Applications*, ed. D Joubert. Berlin: Springer
64. Lamoen D, Ballone P, Parrinello M. 1996. *Phys. Rev. B* 54:5097–105
65. Modinos A. 1984. *Field, Thermionic and Secondary Electron Spectroscopy*. New York: Plenum
66. Harris CB, Ge NH, Lingle RL, McNeill JD, Wong CM. 1997. *Annu. Rev. Phys. Chem.* 48:711
67. Aviram A, Ratner MA. 1974. *Chem. Phys. Lett.* 29:277
68. Waldeck DH, Beratan DN. 1993. *Science* 261:576–77
69. Marcus RA. 1996. *J. Chem. Soc. Faraday Trans.* 92:3905–8
70. Martin AS, Sambles JR, Ashwell GJ. 1993. *Phys. Rev. Lett.* 70:218–21
71. Fischer CM, Burghard M, Roth S, Vonklitzing K. 1994. *Europhys. Lett.* 28:129–34, 375–77
72. Nagesha K, Gamache J, Bass AD, Sanche L. 1997. *Rev. Sci. Instrum.* 68:3883–89

73. Makov G, Nitzan A, Brus LE. 1988. *J. Chem. Phys.* 88:5076–85
74. Ferry DK, Goodnick SM. 1997. *Transport in Nanostructures*. Cambridge, UK: Cambridge Univ. Press
75. Wilkins R, Ben-Jacob E, Jaklevic RC. 1989. *Phys. Rev. Lett.* 63:801–4
76. Andres RP, Bein T, Dorogi M, Feng S, Henderson JI, et al. 1996. *Science* 272:1323–25
77. Kuznetsov AM, Ulstrup J. 1993. *J. Electroanal. Chem.* 362:147–52
78. Fan F-RF, Bard AJ. 1997. *Science* 277:1791–93
79. Malysheva LI, Onipko AI. 1992. *Phys. Rev. B* 46:3906–15
80. Mujica V, Kemp M, Roitberg A, Ratner M. 1996. *J. Chem. Phys.* 104:7296–305
81. Li Y-Q, Gruber C. 1998. *Phys. Rev. Lett.* 80:1034–37
82. Gurvitz SA, Prager YS. 1996. *Phys. Rev. B* 53:15932–43
83. Datta S. 1995. *Electric Transport in Mesoscopic Systems*. Cambridge, UK: Cambridge Univ. Press
84. Wolf EL. 1985. *Principles of Electron Tunneling Spectroscopy*. New York: Oxford Univ. Press
85. Emberly E, Kirczenow G. 2000. *Phys. Rev. B* 61:5740–50
86. Wagner M. 2000. *Phys. Rev. Lett.* 85:174–77
87. Tour JM, Kozaki M, Seminario JM. 1998. *J. Am. Chem. Soc.* 120:8486–93
88. Todorov TN. 1998. *Philos. Mag. B* 77:965–73
89. Büttiker M, Landauer R. 1982. *Phys. Rev. Lett.* 49:1739–42
90. Büttiker M. 1983. *Phys. Rev. B* 27:6178–88
91. Landauer R, Martin T. 1994. *Rev. Mod. Phys.* 66:217–28
92. Hauge EH, Stoveng JA. 1989. *Rev. Mod. Phys.* 61:917–36
93. Nitzan A, Jortner J, Wilkie J, Burin AL, Ratner MA. 2000. *J. Phys. Chem. B* 104:5661–65
94. Galperin M, Nitzan A, Peskin U. Submitted for publication
95. Stipe BC, Rezaei MA, Ho W. 1998. *Science* 280:1732–35
96. Foley ET, Kam AF, Lyding JW, Avouris P. 1998. *Phys. Rev. Lett.* 80:1336–39
97. Gadzuk JW. 1991. *Phys. Rev. B* 44:13466–77
98. Domcke W, Cederbaum LS. 1980. *J. Phys. B* 13:2829–38
99. Wingreen NS, Jacobsen KW, Wilkins JW. 1988. *Phys. Rev. Lett.* 61:1396

99a. Wingreen NS, Jacobsen KW, Wilkins JW. 1989. *Phys. Rev. B* 40:11834

100. Avouris P, Walkup RE. 1989. *Annu. Rev. Phys. Chem.* 40:1989
101. Medvedev ES, Stuchebrukhov AA. 1997. *J. Chem. Phys.* 107:3821–31
102. Xie Q, Archontis G, Skourtis SS. 1999. *Chem. Phys. Lett.* 312:237–46
103. Kuznetsov AM, Vigdorovich MD, Ulstrup J. 1993. *Chem. Phys.* 176:539–54
104. Austin RH, Hong MK, Moser C, Plombon J. 1991. *Chem. Phys.* 158:473–86
105. Sumi H, Kakitani T. 1996. *Chem. Phys. Lett.* 252:85–93
106. Iversen G, Friis EP, Kharkats YI, Kuznetsov AM, Ulstrup J. 1998. *J. Biol. Inorg. Chem.* 3:229–35
107. Schmickler W, Tao N. 1997. *Electrochim. Acta* 42:2809–15
108. Nitzan A. 1979. *Chem. Phys.* 41:163–81
109. Büttiker M. 1988. *IBM J. Res. Dev.* 32:63–75
110. Bixon M, Jortner J. 1997. *J. Chem. Phys.* 107:1470–82, 5154–70
111. Bonča J, Trugman SA. 1995. *Phys. Rev. Lett.* 75:2566–69

111a. Bonča J, Trugman SA. 1995. *Phys. Rev. Lett.* 79:4874–77

112. Yu ZG, Smith DL, Saxena A, Bishop AR. 1999. *Phys. Rev. B* 59:16001–10
113. Heeger AJ, Kivelson S, Schrieffer JR, Su W-P. 1988. *Rev. Mod. Phys.* 60:781–850
114. Ness H, Fisher AJ. 1999. *Phys. Rev. Lett.* 83:452–55
115. Persson BNJ, Baratoff A. 1987. *Phys. Rev. Lett.* 59:339–42

116. Pollard WT, Felts AK, Friesner RA. 1996. *Adv. Chem. Phys.* 93:77–134
117. Okada A, Chernyak V, Mukamel S. 1998. *J. Phys. Chem.* 102:1241–51
118. Segal D, Nitzan A, Davis WB, Wasielewski MR, Ratner MA. 2000. *J. Phys. Chem. B* 104:3817
119. Segal D, Nitzan A, Ratner MA, Davis WB. 2000. *J. Phys. Chem.* 104:2790
120. Redfield AG. 1957. *IBM J. Res. Dev.* 1:19
121. Segal D, Nitzan A. 2001. *Chem. Phys.* In press
122. Bixon M, Jortner J. 1999. See Ref. 1, pp. 35–202
123. Giese B. 2000. *Acc. Chem. Res.* 33:631–36
124. Davis WB, Svec WA, Ratner MA, Wasielewski MR. 1998. *Nature* 396:60–63
125. Caron LG, Perluzzo G, Bader G, Sanche L. 1986. *Phys. Rev. B* 33:3027–38
126. Haiss W, Lackey D, Sass JK, Besocke KH. 1991. *J. Chem. Phys.* 95:2193
127. Meepagala SC. 1994. *Phys. Rev. B* 49:10761
128. Pan J, Jing TW, Lindsay SM. 1994. *Chem. Phys.* 98:4205
129. Vaught A, Jing TW, Lindsay SM. 1995. *Chem. Phys. Lett.* 236:306–10
130. Nagy G. 1996. *J. Electroanal. Chem.* 409:19–23
131. Hong YA, Hahn JR, Kang H. 1998. *J. Chem. Phys.* 108:4367–70
132. Gurevich YY, Pleksov YY, Rotenberg ZA. 1980. *Photo-Electrochemistry*. New York: Consultant Bur.
133. Mosyak A, Nitzan A, Kosloff R. 1996. *J. Chem. Phys.* 104:1549–59
134. Benjamin I, Evans D, Nitzan A. 1997. *J. Chem. Phys.* 106:6647–54
135. Mosyak A, Graf P, Benjamin I, Nitzan A. 1997. *J. Phys. Chem. A* 101:429–33
136. Benjamin I, Evans D, Nitzan A. 1997. *J. Chem. Phys.* 106:1291–93
137. Nitzan A, Benjamin I. 1999. *Acc. Chem. Res.* 32:854–61
138. Peskin U, Edlund A, Bar-On I, Galperin M, Nitzan A. 1999. *J. Chem. Phys.* 111:7558–66
139. Jo SK, White JM. 1991. *J. Chem. Phys.* 94:5761
140. Barnett RN, Landman U, Nitzan A. 1990. *Chem. Phys.* 93:6535–42
141. Sanche L. 1995. *Scanning Microsc.* 9:619
142. Bader G, Chiasson J, Caron LG, Michaud M, Perluzzo G, Sanche L. 1988. *Radiat. Res.* 114:467–79
143. Chernovitz AC, Jonah CD. 1988. *J. Phys. Chem.* 92:5946
144. Rostkier-Edelstein D, Urbakh M, Nitzan A. 1994. *J. Chem. Phys.* 101:8224–37
145. Barnett RN, Landman U, Cleveland CL. 1988. *Chem. Phys.* 88:4420
145a. Rossky PJ, Schnitker J. 1998. *J. Phys. Chem.* 92:4277
146. Tal-Ezer H, Kosslof R. 1984. *J. Chem. Phys.* 81:3967
147. Naaman R, Haran A, Nitzan A, Evans D, Galperin M. 1998. *J. Phys. Chem.* B 102:3658–68
148. Saad Y. 1996. *Iterative Methods for Sparse Linear Systems*. Boston: PWS
149. Staib A, Borgis DJ. 1995. *Chem. Phys.* 103:2642
150. Theil PA, Madey TE. 1987. *Surf. Sci. Rep.* 7:211
151. Halbritter J, Repphun G, Vinzelberg S, Staikov G, Lorentz WJ. 1995. *Electrochim. Acta* 40:1385–94
152. Christoph R, Siegenthaler H, Rohrer H, Wiese W. 1989. *Electrochim. Acta* 34:1011
153. Schmickler W, Henderson DJ. 1990. *Electroanal. Chem.* 290:283
154. Gurney RW. 1935. *Phys. Rev.* 47:479
155. Ueba H. 1991. *Surf. Sci.* 242:266
156. Albano EV. 1982. *Appl. Surf. Sci.* 14: 183
157. Ueno N, Azuma Y, Yokota T, Aoki M, Okudaira KK, Harada Y. 1997. *Jpn. J. Appl. Phys.* 36:5731–36
158. Dimitrov DA, Trakhtenberg S, Naaman

R, Smith DJ, Samartzis PC, Kitsopoulos TN. 2000. *Chem. Phys. Lett.* 322:587–91
159. Kadyshevitch A, Naaman R. 1995. *Phys. Rev. Lett.* 74:3443
160. Kadyshevitch A, Naaman R, Cohen R, Cahen D, Libman J, Shanzer A. 1997. *J. Phys. Chem. B* 101:4085–89
161. Kadyshevitch A, Ananthavel SP, Naaman R. 1998. *Thin Solid Films* 329:357–59
162. Ray K, Ananthavel SP, Waldeck DH, Naaman R. 1999. *Science* 283:814–16
163. Blodgett KB, Langmuir I. 1937. *Phys. Rev.* 51:964
164. Sanche L. 1995. *Phys. Rev. Lett.* 75: 2904
165. Michaud M, Sanche L. 1984. *Phys. Rev. B* 30:6067
166. Space B, Coker DF, Liu ZH, Berne BJ, Martyna GJ. 1992. *Chem. Phys.* 97: 2002
167. Fano U. 1987. *Phys. Rev. A* 36:1929
168. Goulet T, Jung JM, Michaud M, Jay-Gerin JP, Sanche L. 1994. *Phys. Rev. B* 50:5101–9
169. Grifoni M, Hänggi P. 1998. *Phys. Rep.* 304:229–358

Annual Review of Physical Chemistry
Volume 52, 2001

CONTENTS